Preclinical efficacy, safety, and immunogenicity of a COVID-19 vaccine candidate based on a recombinant RBD fusion heterodimer of SARS-CoV-2

Antonio Barreiro*[1,10], Antoni Prenafeta*[1,10], Gregori Bech-Sabat[1], Mercè Roca[1], Eva Perozo Mur[1], Ricard March[1], Luis González[1], Laia Madrenas[1], Júlia Corominas[1], Alex Fernández[1], Alexandra Moros[1], Mercè Molas[1], Thais Pentinat Pelegrin[1], Clara Panosa[1], Alberto Moreno[1], Ester Puigvert Molas[1], Eva Pol Vilarrassa[1], Jordi Palmada[1], Carme Garriga[1], Teresa Prat Cabañas[1], Júlia Vergara-Alert[2], Cristina Lorca-Oró[2], Núria Roca[2], Leira Fernández-Bastit[2], Jordi Rodon[2], Mònica Pérez[2], Joaquim Segalés[3,4], Edwards Pradenas[5], Silvia Marfil[5], Benjamin Trinité[5], Raquel Ortiz[5], Bonaventura Clotet[5,6], Julià Blanco[5,6], Jorge Díaz Pedroza[7], Rosa Ampudia Carrasco[7], Yaiza Rosales Salgado[7], Jordina Loubat-Casanovas[7], Sara Capdevila Larripa[7], Julia Garcia Prado[7,5], Jordi Barretina[7], Marta Sisteré-Oró[8], Paula Cebollada Rica[8], Andreas Meyerhans [8,9], Laura Ferrer[1]

[1]HIPRA. Avda. La Selva, 135, 17170 Amer (Girona), Spain.

[2]Institut de Recerca i Tecnologia Agroalimentàries (IRTA), Centre de Recerca en Sanitat Animal (CReSA, IRTA-UAB), Campus de la UAB, 08193 Cerdanyola del Vallès, Spain.

[3]Universitat Autònoma de Barcelona, CReSA (IRTA-UAB), Campus de la UAB, 08193 Cerdanyola del Vallès, Spain.

[4]Departament de Sanitat i Anatomia Animals, Facultat de Veterinària, UAB, 08193 Cerdanyola del Vallès, Spain.

[5]IrsiCaixa. AIDS Research Institute, Germans Trias i Pujol Research Institute (IGTP), Can Ruti Campus, UAB, 08916 Badalona, Spain.

[6]University of Vic–Central University of Catalonia (UVic-UCC), 08500, Vic, Catalonia, Spain.

[7]CMCiB-IGTP (Comparative Medicine and Bioimage Centre of Catalonia, Germans Trias i Pujol Research Institute), 08916 Badalona, Spain.

[8]Infection Biology Laboratory, Department of Experimental and Health Sciences, Universitat Pompeu Fabra (UPF), 08003 Barcelona, Spain.

[9]ICREA (Catalan Institution for Research and Advanced Studies), Pg. Lluís Companys 23, 08010 Barcelona, Spain.

[10]These authors contributed equally.

*Corresponding authors

Correspondence: antoni.prenafeta@hipra.com; antonio.barreiro@hipra.com

Summary: The current COVID-19 vaccines have been associated with a decline in infection rates, prevention of severe disease and decrease in mortality rates. However, new variants of concern (VoCs) are continuously evolving, making the development of new accessible COVID-19 vaccines essential in order to mitigate the pandemic. Here we present data on preclinical studies in mice of a receptor-binding domain (RBD)-based recombinant protein vaccine candidate (PHH-1V) consisting of an RBD fusion heterodimer containing the B.1.351 and B.1.1.7 SARS-CoV-2 VoCs and formulated with the SQBA adjuvant, an oil-in-water emulsion produced by HIPRA.

BALB/c and K18-hACE2 mice were immunized with different recombinant RBD fusion heterodimer doses, following a two-dose prime-and-boost schedule. Vaccination induced a $CD4^+$ and $CD8^+$ T cell response and RBD-binding antibodies with neutralising activity against various VoCs with a good tolerability profile. Significantly, a 10-µg or 20-µg RBD fusion heterodimer/dose vaccination conferred 100% efficacy, preventing mortality in SARS-CoV-2 infected K18-hACE2 mice. These findings demonstrate the feasibility of this recombinant vaccine strategy.

Keywords: SARS-CoV-2, COVID-19, second-generation vaccines, RBD fusion heterodimer, preclinical, mice.

1. Introduction

In December 2019, the Severe Acute Respiratory Syndrome Coronavirus-2 (SARS-CoV-2) was identified as the etiological agent of the novel Coronavirus disease 2019 (COVID-19). Soon after that, the scientific community and the pharmaceutical industry began focusing on the development of effective COVID-19 vaccines to mitigate the health emergency. Thanks to these efforts, several vaccines are currently available, and more than 8 billion doses have been administered worldwide (December 2021) (WHO, 2021). The decline in new infection rates in many countries coincides with the introduction of vaccines. However, COVID-19 cases continue to emerge, probably due to the appearance and evolution of novel SARS-CoV-2

variants, the decline of immunological protection provided by the current vaccines, and especially the lack of homogenous distribution of COVID-19 vaccines, with only 8.1% of people in low-income countries having received at least one dose (December 2021) (Hannah Ritchie et al., 2020; Mathieu et al., 2021). As the global outbreak continues, the pandemic is far from being over and it is not clear if the available vaccines will be sufficient to revert the situation. Thus, it is still critical to develop second-generation vaccines using different platforms that are effective against novel variants and that could be further used as a booster, particularly to maintain or even enhance immunity against SARS-CoV-2. (Günl et al., 2021; Moyo-Gwete et al., 2021). Moreover, it is of relevance that these novel vaccines can be stored in refrigerated conditions, making them easier to distribute, avoiding more expensive and less available ultra-low temperature storage and transport conditions to ensure their global supply. Currently authorised vaccines, whether approved under emergency use or fully licensed, are based on viral vectors, inactivated viruses, nucleic acid-based vaccines, and protein subunit vaccines (Mellet and Pepper, 2021).

SARS-CoV-2 is a novel betacoronavirus, which belongs to the subfamily *Coronovirinae* within the family *Coronaviridae* and the order *Nidovirales*. The SARS-CoV-2 genome is a positive-sense single-stranded RNA (+ssRNA) molecule. The genome size ranges between 27 and 32 kbp, one of the largest known RNA viruses. The genomic structure of SARS-CoV-2 contains at least six Open Reading Frames (ORFs), encoding for at least four structural proteins, namely: envelope or spike (S) glycoprotein S; membrane (M) proteins, responsible for the shaping of the virions; envelope (E) proteins, responsible for the virions assembly and release; and nucleocapsid (N) proteins, involved in the RNA genome packaging (Alanagreh et al., 2020). The trimeric S glycoprotein of SARS-CoV-2 is the primary target of viral neutralising antibodies and has been the main protein candidate for vaccine development (Vogel et al., 2020). Consistent with SARS-CoV, angiotensin-converting enzyme 2 (ACE2) binding of the S protein allows cellular entry of SARS-CoV-2 viral particles (Zhou et al., 2020). This protein consists of 2

domains, S1 and S2, allowing the binding of the viral particles and cellular entry by fusing with the host cell membrane (Huang et al., 2020). The receptor-binding domain (RBD) (Thr333-Gly526) is found in the S1 domain and it contains a highly immunogenic receptor-binding motif (RBM) that directly interacts with ACE2 and neutralising antibodies (Yi et al., 2020). Therefore, most key mutations are found in the RBM, allowing the virus to adapt and escape the previously developed immunity (Cao et al., 2022; Liu et al., 2020). To date, several SARS-CoV-2 VoCs with key mutations in the S protein have emerged: alpha (B.1.1.7), beta (B.1.351), gamma (P.1), delta (B.1.617.2) and omicron (B.1.1.529) (Plante et al., 2021; WHO 2022, n.d.).

The S protein is the primary target in vaccine development against betacoronaviruses due to its accessibility for immune recognition (Dai and Gao, 2021). It has been reported that two proline substitutions in the original S protein sequence (S-2P) of MERS-CoV, SARS-CoV and HKU1 coronavirus maintain the antigenic conformation (Pallesen et al., 2017). Thus, learning from these previous results, this S-2P design is used in the authorised mRNA-based vaccines Comirnaty® (Pfizer-BioNTech) (Comirnaty smpc 2021, n.d.) and Spikevax® (Moderna) (Spikevax Smpc, 2021), which substitute the residues K986 and V987 for prolines from the original S protein variant. Likewise, the adenoviral vector-based vaccine Jcovden® (Johnson & Johnson) also contains DNA-encoding for the S-2P protein of the SARS-CoV-2 (Jcovden Smpc, 2022 n.d.)

Adjuvanted protein-based subunit vaccines represent an important type of vaccine, yet their development has lagged compared to other platforms due to the need to optimise the manufacturing process for each protein antigen. The most advanced subunit vaccine programme against COVID-19 is the Novavax vaccine (NVX-CoV-2373, marketed as Nuvaxovid®), which is produced in insect cells in combination with a saponin-based adjuvant (Matrix-M) (Keech et al., 2020). This vaccine, which received an EU conditional marketing authorisation in December 2021, consists of the stable full-length S protein in the antigenically optimal prefusion conformation. In addition, the Sanofi-GSK vaccine candidate, known as Vidprevtyn®, consists of soluble prefusion-stabilized S trimers from SARS-CoV-2 produced in

insect cells combined with the AS03 adjuvant (Francica et al., 2021). Both vaccines have been tested in human clinical trials (Goepfert et al., 2021; Keech et al., 2020). Notably, recombinant proteins are competitive vaccine candidates with an adequate safety profile, no risk of genome integration, no live components, and suitable for people with compromised immune systems (Kyriakidis et al., 2021), showing high productivity yields and good stability profiles (Gavi Alliance- Covax collaboration platform, 2021; Kleanthous et al., 2021; Kyriakidis et al., 2021).

Most cloned neutralising antibodies target the RBD in the S1 domain (Piccoli et al., 2020), although there are additional immunogenic epitopes outside this domain (Wang et al., 2020). It has been reported that more than 90% of neutralising antibodies isolated from convalescent patients target the RBD in one-third of cases (Greaney et al., 2021a). Moreover, depleted sera and plasma samples from individuals vaccinated with a 250-µg dose of the mRNA-1273 vaccine showed that up to 99% of neutralising antibodies target the RBD, even though the antigen is based on the whole prefusion spike conformation (Greaney et al., 2021b). Considering that the RBD domain of the S protein directly interacts with the ACE2 receptor, and therefore, RBD-targeting antibodies are not expected to cause antibody-dependent enhancement (ADE), unlike non-neutralising or sub-neutralising antibodies (Lee et al., 2020), these data highlight the importance of RBD in the immune response against SARS-CoV-2 and emphasize its relevance as a powerful and efficient immunogen in vaccine design.

Given the inherent particularities of the S protein, and especially the RBD domain, our team developed a vaccine-candidate platform based on this immunogen. From amongst the tested preliminary vaccine candidates, combined with one or several adjuvants, we finally proceeded with a protein-based subunit vaccine candidate, namely PHH-1V, consisting of a recombinant RBD fusion heterodimer of the B.1.351 and B.1.1.7 variants of SARS-CoV-2 expressed in Chinese hamster ovary (CHO) cells and formulated with the SQBA adjuvant. Specifically, the SQBA adjuvant is an oil-in-water emulsion produced by HIPRA. Thus, the main aims of this study were to assess the safety and efficacy of the PHH-1V vaccine in BALB/c and K18-hACE2-

transgenic mice models, and to characterise the RBD fusion heterodimer antigen and its immunogenicity.

2. Results

2.1. Recombinant RBD fusion heterodimer expression and characterisation

The antigen of the PHH-1V vaccine candidate is a recombinant RBD fusion heterodimer based on the B.1.351 and B.1.1.7 SARS-CoV-2 variants (**Figure 1(A)**). The N-terminal monomer contains the amino acid sequence of the SARS-CoV-2 RBD protein from the B.1.351 (beta) variant, whereas the C-terminal monomer contains the amino acid sequence of the SARS-CoV-2 RBD protein from the B.1.1.7 (alpha) variant. According to the structural modelling, the critical mutations involved in the higher affinity towards the human ACE2 receptor and the immune escape potential of both variants are clearly exposed on the protein surface. The heterodimer is expressed in mammalian CHO cells and is used with the SQBA adjuvant. After expressing the antigen in a bioreactor fed-batch cultivation, it is purified by a downstream process consisting of sequential stages, including depth and tangential filtration, chromatography steps, and sterile filtrations. The final product is a highly purified antigen, as determined by SDS-PAGE and SEC-HPLC (**Figure 1 (B, C)**), suitable for vaccine formulation. Surface plasmon resonance (SPR) analysis showed an affinity constant of 0.099 nM for hACE2 (**Figure 1 (D)**).

2.2. Recombinant RBD fusion heterodimer antigen immunogenicity

2.2.1. RBD-specific binding antibody titres

The mouse strains B6.Cg-Tg(K18-ACE2)2Prlmn/J (K18-hACE2) (Jackson Laboratories, ME, USA) and BALB/c (Envigo, IN, USA) were immunized with different doses of the recombinant RBD fusion heterodimer antigen (group B: 0.04-µg, group C:0.2-µg, group D:1-µg, group E: 5-µg; and group F:20-µg). The prime immunization of BALB/c mice with the PHH-1V candidate induced higher titres of RBD binding antibodies in groups C to F compared to the control (group A, immunized with PBS) on day 21 post first immunization (D21) ($p<0.01$) (**Figure 2 (A)**).

After the prime-boost immunization, all vaccinated groups (B to F) reached higher IgG titres than the control group on D35/D37 (14/16 days after the boost; *p<0.01*). On D35/D37, specific SARS-CoV-2 RBD-binding antibodies were detected in groups B to D in a dose-dependent manner, with significant differences among these groups (*p<0.01*). However, no significant differences were observed among the groups immunized with more than 1 µg of recombinant RBD fusion heterodimer antigen (groups D to F). Thus, the IgG response was saturated from 1-µg immunization. Likewise, the RBD-specific binding antibody titres were also increased in SARS-CoV-2 infected K18-hACE2 mice upon vaccination (group C and D) compared to infected and non-infected PBS-vaccinated mice (groups A and B) (**Figure S1**). Both vaccinated groups had similar RBD-specific antibody titres and were vaccinated with 10 or 20 µg of recombinant protein RBD fusion heterodimer, respectively.

To estimate the type of cellular immune response elicited by the vaccine, the IgG2a/IgG1 ratios were calculated as a surrogate of the Th1/Th2 cellular immune response. The IgG2a/IgG1 ratio of groups E and F was 0.74 and 0.75, respectively, which suggests a balanced Th1/Th2 immunogenic response upon PHH-1V vaccination in mice (**Figure 2 (B)**).

2.2.2. SARS-CoV-2 neutralising antibody titres

SARS-CoV-2 neutralising antibodies titres in sera from BALB/c mice were determined by a pseudovirus-based neutralisation assay (PBNA) against the S protein of different variants on D35/D37 (14/16 days after the boost). Prime-boost immunization of groups C to F induced higher neutralising antibody titres against the S protein of the alpha variant compared to the control group A (*p<0.01*) (**Figure 2 (C)**). No neutralising antibody response was observed in group B, although IgG binding antibodies were detected on D35/D37. The mean neutralising antibody titres observed in groups C and D remained the same since no statistically significant differences were observed. However, vaccination with 5 µg (group E) and 20 µg (group F) of RBD fusion heterodimer antigen induced higher neutralising titres than group C and groups C and D, respectively. Interestingly, high neutralising titres against all the tested variants (alpha,

beta, gamma, and delta) were detected in sera from group F (**Figure 2 (D)**), especially for the alpha, beta and delta variants. On the other hand, the SARS-CoV-2 neutralising antibodies against the original variant (Wuhan) were increased in SARS-CoV-2 infected humanized K18-hACE2 mice upon vaccination (groups C and D) compared to infected and non-infected PBS-vaccinated mice (groups A and B) (**Figure S2**). Notably, the levels of neutralising antibodies were similar between both vaccinated groups.

2.2.3. Cellular immune response upon PHH-1V vaccination of BALB/c mice

The characterization of the antigen-specific response of splenic T cells 14/16 days after the boost immunization was performed by intracellular cytokine staining (ICS) and enzyme-linked immunospot (ELISpot) assays in female BALB/c mice from groups A (control), E and F (vaccinated with 5 µg or 20 µg of recombinant protein RBD fusion heterodimer, respectively). The ICS data indicate that upon stimulation with an RBD peptide pool, splenocytes from group F displayed significant activation of $CD4^+$ T cells expressing IFN-γ ($p<0.01$) and IL-2 ($p<0.05$) compared to the control group (**Figure 3 (A)**). No significant antigen-specific response of $CD4^+$ T cells expressing TNF-α or IL-4 was observed in group F when compared to the control group. Notably, immunization of mice with a lower RBD dose (group E) did not induce IFN-γ , TNF-α, IL-2 or IL-4 producers' memory $CD4^+$ T cells after the *in vitro* restimulation. Furthermore, splenocytes from group F showed activation of $CD8^+$ T cells expressing IFN-γ ($p=0.082$) and IL-2 ($p<0.05$) after the antigen-specific restimulation compared to the control group. Regarding the statistical differences observed between the control group and the group receiving the 5-µg heterodimer/dose, both groups have very low response values, indicating that the finding is biologically irrelevant (**Figure 3 (B)**). No $CD8^+$ T cell response was observed in splenocytes from group E compared to the control group. Hence, considering the T cells expressing any of the analysed Th1 cytokines (IFN-γ, TNF-α and IL-2), group F showed a significantly higher $CD4^+$ T cell response than the control group ($p<0.01$) (**Figure S3**).

The IFN-γ and IL-4 ELISpot assays showed no significant differences between the two doses of recombinant protein RBD fusion heterodimer (group E vs group F) (**Figure 4 (A)**). However, both groups showed a higher percentage of IFN-γ^+ and IL-4^+ spots compared to the control group (*p<0.01*). Importantly, the percentage of IFN-γ^+ and IL-4^+ in group F was similar, denoting a balanced Th1/Th2 response, while the percentage of IL-4^+ spots was significantly higher than IFN-γ^+ spots in group E (*p<0.01*), suggesting a Th2-biased response in mice immunised with 5 µg of recombinant protein RBD fusion heterodimer.

The extracellular cytokine levels were measured by Luminex Multiplex in supernatants from splenocytes stimulated with a pool of peptides from SARS-CoV-2 RBD. The levels of IL-2 (*p<0.05*) and IL-5 (*p<0.01*) were higher in the supernatants from group E splenocytes compared to the control group (**Figure 4 (B)**). Similarly, the levels of IL-5 (*p<0.01*) and TNF-α (*p<0.05*) were statistically higher in group F compared to group A. A tendency towards an increase in the levels of IL-2 (*p=0.062*) was also observed in group F compared to group A.

2.3. Recombinant RBD fusion heterodimer antigen efficacy in K18-hACE2 mice

To analyse the protective efficacy of the PHH-1V vaccine candidate against COVID-19 and the pathogenic outcomes derived from the SARS-CoV-2 infection, K18-hACE2 mice were used as a challenge model. All groups were vaccinated intramuscularly following the two-dose prime-and-boost schedule: 1st dose (prime) on D0 and 2nd dose (boost) on D21. The SARS-CoV-2 challenge was performed on a subset of animals on D35 through intranasal instillation.

2.3.1. Clinical signs and weights post challenge

The primary endpoint for reporting the protective capacity of the vaccine candidates was weight loss and/or mortality post challenge. Survival curves are presented in **Figure 5 (A)**. Clinical signs of the SARS-CoV-2 infection were observed only in the non-vaccinated and infected group (B) on days 5 (3 animals) and 6 (3 animals) post challenge. In all cases, clinical signs led to endpoint criteria and the animals were euthanised. Thus, survival curves were significantly different among the different groups (*p<0.001*). The weekly individual body

weights of each group during the vaccination period and post challenge are shown in **Figures S4 (B)** and **5 (B)**, respectively. The animals from group B experienced remarkable weight loss from D3 post challenge onwards, as expected due to the COVID-19 infection, showing a significantly lower weight compared with vaccinated animals from group D on D5 post challenge (*p<0.05*) and from groups C and D on D6 post challenge (*p<0.01*).

2.3.2. Viral load by genomic RT-qPCR

Total viral RNA was determined in the lungs, nasal turbinate, brain (**Figure 6 (A)**), oropharyngeal samples, trachea, pharynx, spleen and heart (**Figure S5**). Viral RNA was determined by real-time quantitative polymerase chain reaction (RT-qPCR) on D37 (2 days post infection), D39 (4 days post infection), D42 (in males, 7 days post infection) and D43 (in females, 8 days post infection), or at the time of euthanasia in animals reaching endpoint criteria before the scheduled euthanasia day. As it can be seen in **Figure 6 (A)** and **S5**, immunization with both doses of PHH-1V (10 µg or 20 µg of recombinant protein RBD fusion heterodimer), reduced the viral load measured by PCR in the lungs, nasal turbinate, brain, oropharyngeal swabs, trachea, pharynx, spleen and heart after the experimental infection compared to the infected control (group B).

2.3.3. Virus titration from tissue samples determined in Vero E6 cells

Virus titres were determined using a standard 50% tissue culture infectious dose ($TCID_{50}$) assay on positive samples of RT-qPCR. No infectious virus was detected in oropharyngeal swabs, pharynx, spleen and trachea. Regarding heart samples, only one out of the three positive samples by RT-qPCR resulted positive in viral isolation in cell culture (group B on D4). For the other organs, the results are shown in **Figure 6 (B)**. Samples from groups C and D had a significant lower infective viral load in the lungs during the entire the post-challenge period (*p<0.01*) and in the brain on D4 and D7 post challenge (*p<0.01*). In the nasal turbinate, a significant lower infective viral load was observed in group D compared with group B on D2

($p<0.05$) post challenge and there was a tendency towards a decrease in group C on D2 ($p=0.0615$) and group D on D7 ($p=0.0657$) post infection compared to group B.

2.3.4. Histopathology

Histopathological analyses were performed on the nasal turbinate, lungs, skeletal muscle, and brain of all animals. In other non-main target tissues of the virus (spleen, trachea, or heart), 2 animals per group were analysed. No lesions were found in the spleen, trachea, and heart of any of the studied animals. As shown in **Figure 7**, which considers data from all days, the infected non-vaccinated control (group B) had a higher histopathological score in the lungs compared to group C ($p<0.05$), and in the brain compared to group C ($p<0.005$) and D ($p<0.005$). No significant differences between groups were observed in the histopathological score of the nasal turbinate.

2.4. Safety of the recombinant RBD fusion heterodimer antigen after vaccination

The preclinical safety of the PHH-1V candidate vaccine was evaluated on BALB/c mice immunised with different doses of the RBD fusion heterodimer by measuring the bodyweight of each animal once a week until D35/D37. For additional safety information, clinical signs and local reactions were monitored. Differences in bodyweight were observed between the control group and some of the vaccinated groups at different times. The fact that the highest dose (group F) did not show significant differences with the control group during the entire study suggests that these differences in bodyweight are not related to the antigen composition. On the other hand, the differences observed in bodyweight cannot be attributed to the adjuvant because all the PHH-1V vaccines contain the same amount of adjuvant. The mean bodyweight of the control group was above the rest of the groups from the beginning of the study, which could have contributed to the differences observed with the rest of the groups throughout the study (**Figure S4 (A)**). No clinical signs or local reactions were detected after the vaccinations in BALB/c mice.

Additionally, the PHH-1V safety was evaluated in humanised K18-hACE2 mice, and bodyweight and clinical signs were also monitored during the vaccination period. No significant changes in bodyweight were observed between the different groups (**Figure S4 (B)**) and vaccinated animals did not show clinical signs or local reactions. The histological evaluation of the injection site revealed a mild lesion (with multifocal mononuclear inflammatory infiltrates within and around muscular fibres) in one of the hind limbs of 1 animal vaccinated with the 10-µg RBD fusion heterodimer/dose on D2 and 2 animals vaccinates with the 20-µg RBD fusion heterodimer/dose on D4 post challenge (**Figure 7**).

3. Discussion

In this study, the effect of the recombinant protein RBD fusion heterodimer dose on the immunogenicity and safety of the PHH-1V vaccine was tested in BALB/c and K18-hACE2 mice. Furthermore, the preclinical efficacy of the vaccine candidate was also assessed in SARS-CoV-2-infected and non-infected K18-hACE2 mice. We show that the active substance of the PHH-1V vaccine candidate, the RBD fusion heterodimer, is stable and has an affinity constant of 0.099 nM against the human ACE2 receptor, which indicates an outstanding binding affinity with its natural ligand. The whole sequence of the antigen originates from the SARS-CoV-2 RBD domains of the B.1.1.7 (alpha) and B.1.351 (beta) variants, which have been shown by Ramanathan *et al.* (Ramanathan et al., 2021) to bind ACE2 with increased affinity. We were able to obtain the antigen at high purity, which is consistent with its use as an active drug substance in a vaccine. CHO, the expression system selected to produce this antigen, has been a workhorse to produce monoclonal antibodies and other protein-based therapeutic entities for decades (Sharker and Rahman, 2021). It has been fully accepted for this purpose by regulatory agencies worldwide.

The PHH-1V vaccine candidate was shown to be safe in mice since it did not cause clinical signs (general and local) nor was there any bodyweight loss attributable to the vaccine composition in either immunised BALB/c or K18-hACE2 mice. Although the histological evaluation of the

injection sites revealed mild lesions with cellular infiltrates in a few vaccinated animals, these were attributable to the local innate immune response induced upon injection with adjuvant-containing vaccines. Moreover, we have consistently observed an adequate safety profile in other animal species in which the PHH-1V vaccine candidate has been tested, such as rats, rabbits, cynomolgus monkeys and pigs (unpublished data). The SQBA adjuvant used in this vaccine might be related to the good tolerability shown in these animal models.

Regarding the RBD-binding antibodies humoral response, a dose response was observed on D35/D37 upon vaccination with RBD heterodimer doses of 0.04, 0.2 and 1 µg/dose, however, this response saturates with higher immunization doses. Significant total IgG titres were observed after just a single dose for doses of 0.2 µg and above. These results suggest a good potency profile for the antigen included in the PHH-1V vaccine candidate, with similar or superior performance to other previously reported immunogens based on similar platforms (Kuo et al., 2020; Tian et al., 2021). Moreover, potent pseudovirus-neutralising activity against the alpha variant was elicited by the 0.2-µg RBD fusion heterodimer/dose immunization, reaching the highest titres with the 20-µg RBD fusion heterodimer/dose immunization. Furthermore, a robust pseudovirus-neutralising activity of sera from mice immunised with 20 µg of RBD fusion heterodimer/dose was confirmed against the beta, gamma, and delta variants. This cross-reactivity was previously confirmed in earlier exploratory trials, where no significant differences were observed in the pseudovirus-neutralising titres against the alpha, beta, and gamma variants in mice upon vaccination with 20-µg RBD fusion heterodimer/dose (data not shown). Notably, the pseudovirus neutralisation assays from this work were performed in the same laboratory and under identical conditions as those that were previously reported to have a good correlation with live virus neutralisation assays (Trinité et al., 2021) which highlights the biological relevance of the neutralising antibody titres that were obtained. Previous results show that upon vaccination with mRNA-based vaccines (Spikevax® and Comirnaty®), the SARS-CoV-2 neutralisation capacity is significantly decreased against the

gamma and beta variants, even in fully vaccinated individuals. This reduction in neutralisation capacity is similar to the delta variant (Garcia-Beltran et al., 2021; Planas et al., 2021; Wall et al., 2021). Thus, even though the recombinant protein RBD fusion heterodimer was designed to elicit a response against the SARS-CoV-2 alpha and beta variants, our data also demonstrate a further neutralising activity against the delta variant, the dominant variant around the world at the time when the study was designed (Genomic epidemiology of novel coronavirus - Global subsampling, 2021; Hadfield et al., 2018). This is critical to mitigating the current pandemic situation, although further studies will have to confirm our findings in human subjects. Moreover, our antigen contains several mutations that are of high concern, mutations which are present in currently designated VoCs and which could potentially arise in future variants. That includes the E484K substitution present in the beta and B.1.621 (mu) variants, as well as the K417N and N501Y mutations present in the omicron variant. E484K is related to immune escape and reduced antibody neutralisation, compromising the efficacy of currently approved vaccines (Jangra et al., 2021).

Regarding cellular response upon vaccination, the ICS data indicate that immunization with the highest dose of 20-µg RBD fusion heterodimer/dose induced a robust Th1-dominant response with activation of $CD4^+$ and $CD8^+$ T cells expressing IFN-γ and IL-2. Notably, ICS detected no significant IL-4 expression in the splenocytes from immunised animals. However, IL-4 ELISpot assays detected the expression of this Th2 cytokine in splenocytes from both immunised groups. Specifically, according to the ELISpot results, the immunization with the 5-µg RBD fusion heterodimer/dose elicited a Th2-biased response, while the immunization with the 20-µg RBD fusion heterodimer promoted a balanced Th1/Th2 response. These differences in the cytokine expression between both assays might be explained by the differences in the incubation time of the splenocytes after the RBD peptide pool stimulation, which was 48 h for the ELISpot compared to 5 h for the ICS. Furthermore, the experimental conditions (number of splenocytes and incubation time) assayed to detect IFN-γ and IL-4 via ELISpot were different;

hence, these data must be interpreted carefully. Th1 immunity is known to be protective for most infections since it promotes humoral immunity as well as phagocytic and cytotoxic T cell activity, whereas the Th2 response assists with the resolution of inflammation (Spellberg and Edwards, 2001). Based on the ICS data, the immunization with the 20-µg RBD fusion heterodimer/dose seems to induce a polarised Th1 immune response.

Extracellular cytokine production was also measured by Luminex Multiplex in supernatants from splenocytes after 48 h of stimulation, where a balanced production of Th1 (TNF-α, IL-2) and Th2 (IL-5 but no IL-4 nor IL-6) cytokines was found in vaccinated mice. Notably, IFN-γ was not detected by Luminex, probably due to the early expression of this factor and its rapid degradation. Importantly, IL-10 was not detected in the supernatants, which indicates that the immunization with PHH-1V did not elicit an anti-inflammatory response after the restimulation of splenocytes with RBD peptide pools.

The IgG2a/IgG1 ratio was measured to assess Th1/Th2 polarization after the prime-boost immunization. IgG1 is produced during any type of immune response, while IgG2a is mainly produced during a Th1-polarised immune response (Snapper and Paul, 1987). Mice immunised with either the 5-µg or the 20-µg RBD fusion heterodimer/dose induced RBD-binding antibodies of both IgG2a and IgG1 subclasses, with an IgG2a/IgG1 ratio near 0.8, indicating a balanced Th1/Th2 response upon PHH-1V vaccination.

Thus, all the data suggest that PHH-1V immunization with the 20-µg RBD fusion heterodimer/dose elicits a robust $CD4^+$ and $CD8^+$ T cell response with an early expression of Th1 cytokines upon restimulation *in vitro*, and balanced Th1/Th2 cytokine production after 48h post stimulation.

Regarding the preclinical efficacy of the PHH-1V vaccine candidate, it was tested at 2 different doses, 10 µg and 20 µg of RBD fusion heterodimer/dose, in K18-hACE2 mice. Upon the SARS-CoV-2 challenge, vaccinated animals were able to overcome the infection since neither clinical signs nor bodyweight loss was detected. By contrast, all non-vaccinated and infected animals

reached the endpoint criteria on D5 or D6 post challenge and had to be euthanised. Furthermore, this group of animals experienced remarkable weight loss from D3 post challenge onwards due to the SARS-CoV-2 infection. Therefore, our data show 100% efficacy in preventing mortality and bodyweight loss in infected K18-hACE2 mice upon PHH-1V vaccination.

In addition, immunization with either the 10-µg or the 20-µg RBD fusion heterodimer/dose of PHH-1V reduced the viral load measured via qPCR in the lungs, nasal turbinate, and brain in K18-hACE2 mice. The viral load excretion measured in oropharyngeal swabs was also reduced upon challenge in vaccinated animals. Moreover, differences in the viral load after the SARS-CoV-2 challenge between vaccinated animals and infected non-vaccinated control animals were also found in other respiratory (trachea and pharynx) and systemic (spleen and heart) organs. Notably, when RT-qPCR positive samples were titrated to determine the infective viral load, most of the samples of vaccinated animals showed negative results, whereas most of the samples of the infected control group resulted in significantly higher viral loads. Taken together, these results suggest less viral replication in vaccinated mice, which discards antibody-dependent enhancement (ADE) of the infection upon vaccination. Indeed, RBD is known to pose a low potential for risk of ADE because antibodies against this domain block receptor binding (An et al., 2021). Likewise, the histopathological evaluation of tissues from vaccinated mice showed no lesions in the brain and mild lesions in the lungs and nasal turbinate upon SARS-CoV-2 infection. By contrast, infected control mice displayed moderate lesions in the lungs and brain, which is consistent with the high viral loads detected in this group.

Overall, in this study the PHH-1V vaccine has been shown to be safe and immunogenic in mice, inducing RBD-binding and neutralising antibodies. Mice immunised with 20 µg of recombinant protein RBD fusion heterodimer/dose showed neutralising activity against the alpha, beta, gamma, and delta variants. Likewise, immunization with 20 µg of RBD fusion

heterodimer/dose elicited robust activation of $CD4^+$ and $CD8^+$ T cells, producing an early Th1 response upon *in vitro* restimulation. Importantly, vaccination with either the 10-µg or the 20-µg RBD fusion heterodimer/dose prevented weight loss and clinical signs (including mortality) upon SARS-CoV-2 challenge in mice. Both tested doses reduced viral loads in several organs and prevented the infective viral load in the lungs and brain upon experimental infection. In addition, immunization with 20 µg of RBD recombinant protein fusion heterodimer reduced the infective viral load in the upper respiratory tract (nasal turbinate). Most importantly, besides the efficacy and safety features of PHH-1V, this second-generation COVID-19 vaccine is easy to adapt to potential emergent SARS-CoV-2 variants, allowing for the inclusion of up to 2 different RBDs to generate cross-immunity against novel emergent variants. The PHH-1V vaccine candidate showed promising preclinical data and is currently being evaluated in Phase I/IIa (NCT05007509), Phase IIb (NCT05142553) and Phase III (NCT05246137) clinical trials (U.S. National Library of Medicine, 2021).

4. Acknowledgements: We would like to thank Marta Ribó, Ariadna Pararols, Rubén Hernández and Helena Sánchez for their assistance in the animal care; Jèssica Gómez and Maria Bosch for their support in the tabulation of raw data; Anna Moya, Mireia Muntada, Lidia Galindo and Núria Elias for the ELISA analysis and protein characterization; Manuel Cañete for his support in the statistical analysis; Marta Bau for her assistance in the production of the vaccine antigen; Claudia Millán for helping with the modelling and visualization of the heterodimeric RBD structure; David Solanes Foz for his support to the ABSL3 Unit; the CMCiB Ethical Committee members (Jorge Carrillo, Eulàlia Genescà, Carol Galvez, Carol Soler and Patricia Fachal) for their support on the ethical review of animal procedures; the IGTP Biosafety Committee members (Pere-Joan Cardona, Julià Blanco, Meritxell Carrió, Natalia Ruiz, David Izquierdo and Noemí Parraga) for their support on the review biosafety procedures; Glòria Pujol and Eduard Fossas for their assistance in the revision of the manuscript; and Francisco Díaz-Sáez and Anna Muñoz from Alta Medical Services for providing medical writing

support. We gratefully acknowledge editorial support from Sarah Marshall. This project was partially funded by the Centre for the Development of Industrial Technology (CDTI, IDI20210115), a public organisation answering to the Spanish Ministry of Science and Innovation.

5. Author Contributions: Conceptualization, Investigation, Methodology, Resources, Formal Analysis and Data Curation: A.B., A.P., L.F., L.M., J.C., A.F., A.Mo., M.M., G.B., E.P.M., M.R., R.M., L G., E.P.M., E.P.V., J.P., C.P., T.P.P. & A.M.; Writing Original Draft, Writing – Review & Editing, Visualization and Supervision: A.B. & A.P.; Investigation: J.R., N.R., M.P., C.L.-O., J.V-A., L.F.-B., J.S., E.P., S.M., B.T., R.O., P.C.R., M.S.-O., J.D., R.A., Y.R. & J.L-C.; Resources: J.V.-A., C.L.-O., J.S., B.T., B.C., J.B., A.M., J.D., Y.R. & S.C.; Writing – Review & Editing: A.Mo, J.V.-A., C.L.-O., J.S., E.P., B.T., B.C., J.B., A.M., J.D., S.C., J.G-P & J.B.; Supervision: J.V.-A., J.S., B.C., J.B., A.M., J.G.-P. & J.B.; Project Administration: L.F.; Conceptualization: T.P.C. & C.G.

6. Competing Interests: Authors indicated as "1" are employees of HIPRA, a private pharmaceutical company that develops and manufactures vaccines. CReSA, IrsiCaixa, CMCiB-IGTP, UPF and ICREA have received financial support from HIPRA. Several patent applications have been filed by HIPRA SCIENTIFIC S.L.U. and Laboratorios HIPRA, S.A. on different SARS-CoV-2 vaccine candidates and SARS-CoV-2 subunit vaccines, including the novel recombinant RBD fusion heterodimer PHH-1V. These patent applications are not yet public. Antonio Barreiro, Antoni Prenafeta, Luis González, Laura Ferrer, Esther Puigvert, Jordi Palmada, Maria Teresa Prat and Carmen Garriga are the inventors of these patent applications.

7. Figure Legends

Figure 1. Structure and characterisation of the B.1.351 (beta) - B.1.1.7 (alpha) RBD receptor-binding domain (RBD) heterodimer, immunogen of PHH-1V. (A) Structural representation of the RBD heterodimer. Top: sequence diagram. Bottom left: front view of the RBD heterodimer cartoon structure. Bottom right: top view of the antigen surface structure. Mutations are highlighted in green (K417N), cyan (E484K) and yellow (N501Y). **(B)** SDS-PAGE. The reduced

and non-reduced purified antigens were loaded at three serial dilutions: 1/10, 1/20 and 1/40. M: molecular weight ladder. C: BSA control. **(C)** SEC-HPLC chromatogram of the purified antigen. **(D)** Surface plasmon resonance (SPR) for the quantitative evaluation of the affinity between the antigen and its natural ligand, the human ACE2 receptor. RU: resonance units.

Figure 2. Analysis of the antibody response upon PHH-1V vaccination in mice. (A) SARS-CoV-2 RBD-specific IgG responses in groups A to F on days D0, D21 and D35/D37**.** Endpoint antibody titres determined by ELISA in female BALB/c mice are shown. Each data point represents an individual mouse serum, with bars representing the mean titre and the corresponding standard deviation (SD). **(B)** Endpoint titre ratios of IgG2a to IgG1 in female mice vaccinated with PHH-1V vaccine (groups E and F). Analyses of IgG1 and IgG2 subclasses in groups E and F were performed by ELISA on serum samples taken on day D35/D37. **(C)** Neutralising antibody responses in groups A to F. SARS-CoV-2 neutralising antibody titres in sera, against pseudoviruses that express the S protein with the α sequence, were determined by PBNA 14/16 days after the second dose of each vaccine (D35/D37). Sera from female BALB/c mice collected on D35/D37 were assessed for pseudovirus-neutralising activity. Titres are expressed as $\log_{10}$ IC_{50}. Data were analysed using a generalized least squares (GLS) model on the $\log_{10}$-transformed values. For comparison against groups A and B, one-sample *t*-tests on the estimated marginal means were used against the null $H_0 = 1.78$ (indicated with lower case letters if significant). **(D)** Neutralising antibody responses against multiple SARS-CoV-2 variants (α, β, ɣ, δ) by PBNA upon 20-µg RBD fusion heterodimer/dose immunization. Sera from group F mice collected on D35/D37 were assessed for pseudovirus-neutralising activity. Titres are expressed as $\log_{10}$ IC_{50}. Data represent the mean titre ± SD. * $p<0.05$; ** $p<0.01$; $^{+}$ $0.05<p<0.1$. Data from female mice are shown. See also Figures **S1, S2** and **S6**.

Figure 3. PHH-1V-induced $CD4^+$ and $CD8^+$ T cell responses. Splenocytes from vaccinated female BALB/c mice were isolated 14/16 days after boost immunization (D35/D37), stimulated with RBD peptide pools, and analysed by intracellular cytokine staining. The frequencies of

cytokine expressing $CD4^+$ T cells (**A**) and $CD8^+$ T cells (**B**) are shown. The cytokine expression in splenocytes stimulated with the medium was considered the background value and this was subtracted from peptide-specific responses. Group A (n=8; controls), immunized with PBS; group E (n=8), immunized with 5 µg/dose of PHH-1V; and group F (n=8), immunized with 20 µg/dose of PHH-1V. Data represent the mean ± SD. ** $p<0.05$; ** $p<0.01$; $^+$ $0.05<p<0.1$.* Data from female mice are shown. See also **Figures S3** and **S6**.

Figure 4. Frequencies of PHH-1V-induced IFN-γ and IL-4 responses, and extracellular cytokine levels in vaccine-induced splenocytes from mice. (A) Splenocytes from vaccinated BALB/c mice were isolated 14/16 days after boost immunization (D35/D37), stimulated with RBD peptide pools, and analysed by IFN-γ and IL-4-specific ELISpot assays. Each data point represents an individual mouse. **(B)** Extracellular cytokines were measured by Luminex Multiplex in supernatants from BALB/c splenocytes stimulated with a pool of peptides from SARS-CoV-2 RBD. Cytokine levels in splenocytes stimulated with the medium were considered the background value and these were subtracted from the responses measured from the RBD peptide pool for each individual mouse. Data were analysed using Kruskal-Wallis' H test and Dunn's post-hoc with Holm's correction for multiple testing. Groups in lower case letters were compared using Mann-Whitney's test. Data represent the mean ± SD. ** $p<0.05$; ** $p<0.01$; $^+$ $0.05<p<0.1$*. Data from female mice are shown.

Figure 5. Survival and bodyweight loss in vaccinated and non-vaccinated mice upon SARS-CoV-2 challenge. (A) Survival curves for groups of immunized K18-hACE2 mice with PHH-1V vaccine and control groups. Group A (n=8, 4F + 4M), group B (n=18, 9F + 9M), group C (n=18, 9F + 9M), and group D (n=18, 9F + 9M). Survival analysis (Kaplan-Meier estimates and log-rank test to compare groups) was performed to study differences in time to/before clinical signs and mortality. Asterisks represent censored data (i.e. animals leaving the study; in this case, it represents selected animals that were euthanised for serial necropsies). **(B)** Mean weight change after SARS-CoV-2 challenge calculated as a percentage of the pre-challenge weight in

K18-hACE2 mice. Group A (n=8, 4F + 4M), group B (n=18, 9F + 9M), group C (n=18, 9F + 9M), and group D (n=18, 9F + 9M). Data represent the mean ± SD. ** p<0.05; ** p<0.01.* $^{+}$ *0.05<p<0.1*. DPI: days post infection. See also **Figures S4** and **S6**.

Figure 6. SARS-CoV-2 viral load and viral titration in Vero E6 cells from lung, nasal turbinate and brain samples ($TCID_{50}$/mL) from mice. (A) SARS-CoV-2 RT-qPCR (number of copies) in the lungs, nasal turbinate and brain, collected from challenged animals. **(B)** Viral titres were determined using a standard $TCID_{50}$ assay on positive samples of RT-qPCR (in some exceptional cases, RT-qPCR and viral isolation were performed in parallel for logistical reasons). RT-qPCR-negative samples are represented as 0 $TCID_{50}$/mL. The detection limit was set at 1.8 $TCID_{50}$/mL. Data represent the mean ± SD. ** p<0.05; ** p<0.01;* $^{+}$ *0.05<p<0.1*. DPI: days post infection. See also **Figure 6**.

Figure 7. Histopathology score in the lungs, nasal turbinate, brain, and hind limb skeletal muscle stained with H&E from K18-hACE2 mice samples at endpoint days. (**A**) Histopathological analyses from the lungs, nasal turbinate, and brain were determined for all animals. Hind limb skeletal muscle analysis was determined for 2 animals per group. For each tissue sample, lesions were classified as follows: multifocal broncho-interstitial pneumonia; multifocal lymphoplasmacytic rhinitis; multifocal lymphoplasmacytic meningoencephalitis; and multifocal mononuclear inflammatory infiltrates within and around muscular fibres. Lesions were evaluated with the following score: 0 (no lesion); 1 (mild lesion); 2 (moderate lesion); and 3 (severe lesion). Samples scheduled for day 7 from groups A, C and D correspond to D7 (for males) or D8 (for females); samples of group B were taken on D5 (n=3) or D6 (n=3), when animals reached the endpoint criteria, and are represented on D7. Data represent the mean ± SD. *** p<0.01*. DPI: days post infection. (**B**) Representative images of brain and lung lesions of studied hACE2-transgenic mice showing scores of 0 (lack of lesions), 1 (mild lesions), and 2

(moderate lesions). None of the animals of the study showed lesions with score 3 (severe lesions).

8. STAR Methods

RESOURCE AVAILABILITY

Lead contact

Requests for further information or data should be directed to and will be fulfilled by the lead contact, Antoni Prenafeta (antoni.prenafeta@hipra.com).

Materials availability

There are restrictions to the availability of the SARS-CoV-2 protein recombinant RBD heterodimer and PHH-1V vaccine due to patents not being public yet. Additionally, project-related biological samples are not available since they may be required by Regulatory Agencies or by HIPRA during the clinical development of the vaccine.

Data and code availability

- Data reported in this study cannot be deposited in a public repository because patents are not yet public, and the vaccine is under clinical evaluation. Upon request, and subject to review, the lead contact will provide the data that support the reported findings.
- This paper does not report original code.
- Any additional information required to reanalyse the data reported in this paper is available from the lead contact upon request.

EXPERIMENTAL MODEL AND SUBJECT DETAILS

Animals

BALB/c mice (Envigo, #162) and B6.Cg-Tg(K18-ACE2)2Prlmn/J (K-18-hACE2) transgenic mice (Jackson Laboratories, #034860) were used as animal models. All procedures that involved BALB/c mice were conducted in accordance with the European Union Guidelines for Animal

Welfare (Directive 2010/63/EU) and approved by the Ethics Committee of HIPRA Scientific S.L.U. and the Department of Territory and Sustainability of the Catalan Government (file: 11388). The experimental procedure that involved the use of K18-hACE2 mice was conducted in accordance with the European Union Guidelines for Animal Welfare (Directive 2010/63/EU) and was approved by the CMCiB Ethics Committee and the Department of Territory and Sustainability of the Catalan Government (file: 11490). The animal study design followed the principles of the 3Rs and animal welfare.

Forty-eight 5-week-old female BALB/c mice were allocated to 6 groups (n=8) and were used for safety and immunogenicity assays. Group A was vaccinated with PBS; group B was immunised with the 0.04-µg recombinant protein RBD fusion heterodimer/dose; group C was immunised with the 0.2-µg recombinant protein RBD fusion heterodimer/dose; group D was immunised with the 1-µg recombinant protein RBD fusion heterodimer/dose; group E was immunised with the 5-µg recombinant protein RBD fusion heterodimer/dose; and group F was immunised with the 20-µg recombinant protein RBD fusion heterodimer/dose. These animals were monitored daily for clinical signs and bodyweight was recorded weekly until D35/D37; at that time, the animals were euthanised and tissues were collected. Animals were watered and fed *ad libitum* with Premium Scientific Diet SAFE® A04 (Safe-lab). Animals were kept on Arbocel® small functional cellulose pellets (Rettenmaier Ibérica, S. L.) with a light/dark cycle of 12 h at a 22 ºC ± 2 ºC in optimum hygienic SPF conditions behind a barrier system under positive pressure with 37 air room renovations per hour. The animals were housed in a stainless-steel rack with polycarbonate cages (530 x 280 x 150 mm) with stainless steel covers equipped with environmental enrichment (nest material: cellulose paper and wood-wool, one PET roll and a PET plastic enrichment dome and a red translucent wheel). The animals were identified with a cage card and individual fur dye. A precision scale (Sartorius, model 112, 6.1 kg with 0.01 g resolution) was used to record the animals' weights.

For further safety, immunogenicity, and efficacy assays, 62 (31F + 31M) 4/5-week-old K18-humanised ACE2 (hACE2) mice were allocated to 4 groups (n=18; 9F + 9M, except for the placebo group: n=8; 4F + 4M). Specifically, group A was intramuscularly injected with PBS and non-infected; group B was injected with PBS and infected with SARS-CoV-2; group C was vaccinated with 10 µg/dose of recombinant protein RBD fusion heterodimer and infected with SARS-CoV-2; and group D was vaccinated with 20 µg/dose of recombinant protein RBD fusion heterodimer and infected with SARS-CoV-2. Animals from satellite subgroups were euthanised on D35 to assess the immunological response of the vaccinated group. Challenged animals were chronologically euthanised on D37, D39 and D42 (males)/D43 (females). Several tissue samples were collected for further analyses. Animals were watered and fed *ad libitum* with Teklad Global 16% Protein Rodent Diet (Envigo, #2916). Animals were kept on cellulose pellets from Rettenmaier Ibérica. Animals were housed in a ventilated rack, model Blue Line Next/Boxunss (Tecniplast, #1145T00SUV-CP), equipped with environmental enrichment (nest material: cellulose paper and cardboard roll). Animals were kept with a light/dark cycle of 12h at 22 ºC ± 2 ºC, with negative room pressure and 20 air renovations per hour. The animals were identified with a dorsal subcutaneous microchip (Trovan, #ID100-B 1.4 Mini transponder). A reader with an integrated scale (Trovan, model 2812005) was used to record the animals' weights. Cibertec was used as the anaesthesia equipment.

In order to comply with animal welfare regulations, all animals were injected with a 0.1 mL/dose of the test vaccine, distributed equally in both hind legs (2 x 50 µL). Animals from satellite subgroups were euthanised on D35 to assess the immunological response of the vaccinated group. Vaccines were injected intramuscularly following a two-dose prime-and-boost schedule: 1st dose (prime) on D0 and 2nd dose (boost) on D21. The SARS-CoV-2 challenge was performed through intranasal inoculation with the strain SARS-CoV-2 Catalonia 02 on a subset of animals on D35 with 25 µL in each nostril (10^3 $TCID_{50}$/mice in 50 µL/mice). This strain (GISAID ID: EPI_ISL_471472), which included the following mutations compared to

Wuhan strain, D614G (Spike), K837N (NSP3), P323L (NSP12), was isolated from a male patient from Barcelona, who showed respiratory symptoms. The intranasal experimental infection was performed under sedation with isoflurane 4-5%. BALB/c mice vaccination and sampling were performed at HIPRA (Girona, Spain). K18-hACE2 mice vaccination, SARS-CoV-2 challenge, and sampling were performed in the ABSL3 unit of the Comparative Medicine and Bioimage Centre of Catalonia of the Germans Trias i Pujol Research Institute (Badalona, Spain). The protocol followed is depicted in **Figure S6**.

Cell lines

HEK293T cells overexpressing WT human ACE-2 (Integral Molecular, USA) were used as target in the pseudovirus-based neutralisation assay. Cells were maintained in T75 flasks with Dulbecco's Modified Eagle's Medium (DMEM) supplemented with 10% FBS and 1 µg/mL of Puromycin (Thermo Fisher Scientific, USA).

Expi293F cells (Thermo Fisher Scientific) are a HEK293 cell derivative adapted for suspension culture, which were used for SARS-CoV-2 pseudovirus production. Cells were maintained under continuous shaking in Erlenmeyer flasks following the manufacturer's guidelines.

Vero E6 (ATCC CRL-1586) cell monolayers were cultured for 3 days at 37 ºC and 5% CO2 in DMEM (GIBCO) supplemented with 100 U/mL penicillin, 100 µg/mL streptomycin and 2 mM glutamine (all reagents from Thermo Fisher Scientific). CHO cells were cultured in a bioreactor in a chemically defined media, at 36-38 ºC with a pH 6.80 - 7.40, 5-8% CO_2 for 60-108 hours with stirring (tip speed 0.4-1) and glucose 2-9 g/L.

METHOD DETAILS

Recombinant RBD fusion heterodimer characterisation

The antigen was produced in a bioreactor based on a selected stable CHO-clone. A fed-batch strategy was used for high-cell-density cultivation and expression of the RBD fusion heterodimer. Upon harvest, the cell broth was clarified by depth filtration. The clarified supernatant was further purified via sequential chromatography. The purified antigen was

then buffer exchanged by tangential flow filtration and filter sterilised. Purity and integrity were evaluated by SDS-PAGE with Bolt™ 4 to 12% Bis-Tris gels (Thermo Fisher, ref. NW04120BOX), stained with One-Step Blue Protein Gel Stain (Biotium, ref. 21003), and by SEC-HPLC with an Xbridge Protein BEH SEC (Waters, ref. 186009160) connected to an HP1100 system (Agilent Technologies).

The affinity test of the RBD heterodimer with human ACE2 by surface plasmon resonance (SPR) was performed by ACROBiosystems. The Fc-tagged ACE2 (AC2-H5257, ACROBiosystems) was immobilised in a Series S Sensor Chip CM5 (Cytiva) on a Biacore T200 (Cytiva) using the Human Antibody Capture Kit (Cytiva). The affinity measure was obtained using 8 different RBD heterodimer concentrations. The antigen structure simulations were performed with UCSF ChimeraX (Pettersen et al., 2021).

SARS-CoV-2 recombinant protein RBD heterodimer adjuvanted vaccines

The purified RBD fusion heterodimer was formulated with the SQBA adjuvant, an oil-in-water emulsion produced by HIPRA. The PHH-1V vaccine was tested at different concentrations: 0.04 µg, 0.2 µg, 1 µg, 5 µg and 20 µg of RBD fusion heterodimer/dose for the safety and immunogenicity assays in BALB/c mice. For efficacy assessment in the K18-hACE2 mice animal model, the vaccine was tested at 10 µg and 20 µg of fusion heterodimer/dose. The placebo vaccines were prepared with phosphate-buffered saline (PBS).

Analysis of SARS-CoV-2-specific antibodies

Serum binding antibodies against SARS-CoV-2 RBD were determined by ELISA (HIPRA). MaxiSorp plates (Nunc, Roskilde, Denmark) were coated with 100 ng/well RBD protein (Sino Biologicals, Beijing, China) and blocked with 5% non-fat dry milk (Difco™ Skim Milk, BD, Franklin Lakes, NJ, USA) in PBS. Wells were incubated with serial dilutions of the serum samples and the bound total IgG specific antibodies were detected by peroxidase-conjugated Goat Anti-Mouse IgG (Sigma-Aldrich, St. Louis, MO, USA. Finally, wells were incubated with K-Blue Advanced Substrate (Neogen, Lansing, MI, USA) and the absorbance at 450 nm was

measured using a microplate reader (Versamax microplate reader, Molecular Devices, San Jose, CA, USA). The mean value of the absorbance was calculated for each dilution of the serum sample run in duplicate. Isotypes IgG1 and IgG2a were detected using Peroxidase AffiniPure Goat Anti-Mouse IgG, Fcγ subclass 1 specific, and Peroxidase AffiniPure Goat Anti-Mouse IgG, Fcγ subclass 2a specific, (Jackson ImmunoResearch, Cambridge, UK), respectively. The endpoint titre of RBD-specific total IgG binding antibodies was established as the reciprocal of the last serum dilution that gave 3 times the mean optical density of the negative control of the technique (wells without serum added).

Pseudovirus neutralisation assay

Neutralising antibodies in serum against SARS-CoV-2 Wuhan (original sequence) and the alpha, beta, gamma, and delta variants were determined by a pseudoviruses-based neutralisation assay (PBNA) at IRSICaixa (Barcelona, Spain), using an HIV reporter pseudovirus that expresses the S protein of SARS-CoV-2 and luciferase. Pseudoviruses were generated as described by Pradenas *et al*. (Pradenas et al., 2021). For the neutralisation assay, 200 $TCID_{50}$ of pseudovirus supernatant was preincubated with serial dilutions of the heat-inactivated serum samples for 1 h at 37 °C and then added onto ACE2 overexpressing HEK293T cells. After 48 h, cells were lysed with britelite plus luciferase reagent (PerkinElmer, Waltham, MA, USA). Luminescence was measured for 0.2 s with an EnSight multimode plate reader (PerkinElmer). The neutralisation capacity of the serum samples was calculated by comparing the experimental RLU calculated from infected cells treated with each serum to the max RLUs (maximal infectivity calculated from untreated infected cells) and min RLUs (minimal infectivity calculated from uninfected cells) and expressed as the neutralisation percentage: neutralisation (Trinité et al., 2021) (%) = (RLUmax–RLUexperimental)/(RLUmax–RLUmin) * 100. IC_{50} were calculated by plotting and fitting neutralisation values and the plasma dilution log to a 4-parameters equation in Prism 9.0.2 (GraphPad Software, USA).

Intra-cellular cytokine staining (ICS)

The ICS was performed by the Infection Biology Group at the Department of Experimental and Health Sciences, Universitat Pompeu Fabra (DCEXS-UPF, Barcelona, Spain). Spleens from female mice were mechanically disrupted onto a 40-µM cell strainer and incubated in 5 mL of 0.15 M ammonium chloride buffer for 5 min at room temperature (RT) for red blood cell lysis. Cells were then washed in RPMI (Gibco, Tavarnuzze, Italy) supplemented with 10% FBS, 1% penicillin/streptomycin, 0.05 mM-Mercaptoethanol and 1 mM sodium pyruvate (cRPMI). Two million splenocytes per well (96-well plate) were stimulated in vitro under three conditions: (i) a 1:1 mix of the peptide libraries (PepMix™) from the B.1.1.7 (alpha variant) and B.1.351 (beta variant) lineages covering the entire RBD of the SARS-CoV-2 S protein; (ii) cRPMI (negative control); and (iii) PMA + Ionomycin (positive control) for 5 h at 37 ºC 5% CO_2 in cRPMI in the presence of Brefeldin A (Sigma-Aldrich) for the last 3 h before antibody staining. The final concentrations used were 1 µg/mL of each peptide of the RBD peptide pool, 15 ng/mL of PMA (Sigma-Aldrich) and 250 ng/mL of ionomycin (Sigma-Aldrich). For flow cytometric analysis, equal numbers of cells were stained with Fixable Viability Stain 780 (BD Biosciences, New Jersey, NJ, USA) in PBS for 15 min at RT followed by staining with antibodies against CD3, CD4, CD8 and CD44 for 20 min on ice in FACS buffer (PBS: 5% FCS, 0.5% BSA, 0.07% NaN3). Cells were then fixed for 20 min on ice with 2% formaldehyde and stained with antibodies against intracellular proteins (IFN-γ, TNF-α, IL-2 and IL-4) for 20 min on ice in perm/wash buffer (PBS: 1% FCS, NaN3 0.1%, saponin 0.1%). All antibodies were purchased from either BD Biosciences, Thermo Fisher or BioLegend (see Table S1 for more details). Samples were processed on an Aurora analyser (Cytek, Fremont, CA, USA). FACS data were analysed using FlowJo 10 software (Tree Star Inc., Ashland, OR, USA). The stain index was calculated by subtracting the mean fluorescence intensity (MFI) of the unstained or fluorescence minus one (FMO) control from the MFI of the stained samples and dividing it by two times the standard deviation of the

unstained population. Background cytokine expression in the no-peptide (cRPMI) condition was subtracted from that measured in the RBD peptide pool for each mouse.

Mouse cytokine assay

The cytokine assay was performed by the Infection Biology Group at the Department of Experimental and Health Sciences, Universitat Pompeu Fabra (DCEXS-UPF, Barcelona, Spain). Splenocytes from female mice were seeded at 1.1×10^6 cells/well in 24-well plates and stimulated with a 1:1 mix of the RBD overlapping peptides from B.1.1.7 (alpha variant) and B.1.1351 (beta variant) lineages (1 µg/mL each). cRPMI media was used as a negative control and PMA (15 ng/mL) + ionomycin (250 ng/mL) as a positive control. The supernatants were harvested after 48 h incubation at 37 °C and a panel that quantifies the cytokines IL-2, IL-4, IL-5, IL-6, IL-10, IFN-γ and TNF-α (Luminex Multiplex, Invitrogen, Waltham, MA, USA) was run according to the manufacturer's instructions. These measurements were performed at Veterinary Biochemical Service, Veterinary Faculty, Universitat Autònoma de Barcelona (UAB, Barcelona, Spain).

IFN-γ and IL-4 ELISpot assays

ELISpot assays were performed with mouse IFN-γ and IL-4 ELISpot PLUS kits according to the manufacturer's instructions (3321-4HPT-10 and 3311-4HPW-10, Mabtech, Herndon, VA, USA). A total of 2.5×10^5 or 4×10^5 splenocytes from female mice were seeded per well for the IFN-γ and IL-4 tests, respectively, and *ex vivo* stimulated either with the 1:1 mix of the RBD overlapping peptides from the B.1.1.7 (alpha variant) and B.1.351 (beta variant) lineages (1 µg/mL each), or with complete cRPMI (negative control) or with concanavalin A (5 µg/mL (Sigma-Aldrich)) (positive control). Each condition was run in duplicates. After an incubation period of 18-20 h (for IFN-γ) or 48 h (for IL-4), the plates were manipulated according to the manufacturer's instructions. Spots were counted under a dissection microscope. Frequencies of IFN-γ or IL-4-secreting cells were expressed as the number of responding cells per million

splenocytes. The number of spots in unstimulated cultures (negative control) was subtracted from the spot count in RBD-stimulated cultures.

SARS-CoV-2 genomic RT-qPCR

Total viral load in respiratory tissue samples was determined by RT-qPCR (CReSA, IRTA-UAB, Barcelona, Spain), according to the method described by Brustolin *et al.* (Brustolin et al., 2021c). Viral RNA was extracted from target organs and swabs samples using the IndiMag pathogen kit (Indical Bioscience) on a Biosprint 96 workstation (QIAGEN) according to the manufacturer's instructions. The RT–qPCR used to detect viral gRNA was based on the one published by Corman *et al*. (Corman et al., 2020), with minor modification to adapt it to the AgPath-ID One-Step RT–PCR Kit (Life Technologies). RT–qPCR targets a portion of the envelope protein gene (position 26,141–26,253 of GenBank NC_004718). The primers and probes used, and their final concentration, were the following: forward, 5'-ACAGGTACGTTAATAGTTAATAGCGT-3' [400 nM]; reverse, 5'-ATATTGCAGCAGTACGCACACA-3' [400 nM]; probe, 5'-FAM-ACACTAGCCATCCTTA CTGCGCTTCG-TAMRA-3' [200 nM]. Thermal cycling was performed at 55 °C for 10 min for reverse transcription, followed by 95 °C for 3 min, and then 45 cycles of 94 °C for 15 s plus 58 °C for 30 s.

Virus titration in Vero E6 cell

Virus titres were determined using a standard $TCID_{50}$ assay in Vero E6 cells at CReSA (IRTA-UAB), according to the method described by Brustolin *et al.* (Brustolin et al., 2021) RT-qPCR positive samples were evaluated for infectious virus by titration in Vero E6 cells as previously described (Rodon et al., 2019; Vergara-Alert et al., 2017). Briefly, each sample was 10-fold diluted in duplicate, transferred in a 96 well plate with a Vero E6 cells monolayer and incubated at 37 °C and 5% CO_2. Plates were monitored daily under the light microscope and wells were evaluated for the presence of CPE at 5 dpi. The amount of infectious virus was calculated by determining the $TCID_{50}$ using the Reed–Muench method.

Histopathology

Histopathological analyses were performed at CReSA (IRTA-UAB). Upper (nasal turbinate) and lower (lungs) respiratory tract, and brain were fixed in 10% buffered formalin and routinely processed for histopathology. Haematoxylin- and eosin-stained slides were examined under optical microscope. Multifocal broncho-interstitial pneumonia, multifocal lymphoplasmacytic rhinitis and non-suppurative meningoencephalitis were evaluated from lung, nasal turbinate and brain lesions, respectively, according to the following semi-quantitative score: 0 (no lesion); 1 (mild lesion, multifocal distribution and less than 10% of tissue affected); 2 (moderate lesion, multifocal distribution and between 10-40% of tissue affected); and 3 (severe lesion, multifocal to diffuse distribution and more than 40% of tissue affected) (Brustolin et al., 2021; Vidal et al., 2021). A European certified (ECVP) pathologist A European certified (ECVP) pathologist PA European certified (ECVP) pathologist performed a blinded pathology assessment.

QUANTIFICATION AND STATISTICAL ANALYSIS

Statistical analyses and plots were generated using R (version 4.0.5), SPSS (version 22) or GraphPad Prism (version 9). Unless otherwise specified, all plots depict individual data points for each animal, along with the sample mean and standard deviation. When required, data is either $\log_{10}$- or arcsine-transformed (i.e. log-normal and percentage variables, respectively). The exact number (n) used in each experiment, generally 8-18 animals per group, is indicated in the caption below each figure. For testing the effect of a single factor (i.e. group or viral strain), one-way ANOVA was used when normality can be assumed based on distribution histograms and the Shapiro-Wilk test. Only when the assumption of homoskedasticity was not satisfied (as verified using Levene's test) was Welch's ANOVA performed. Otherwise, data violating the assumption of normality, as well as ordinal variables, were analysed using the Kruskal-Wallis test. For post-hoc pairwise comparisons, different tests were employed depending on the nature of the data and the planned comparisons to perform. Accordingly,

Tukey's HSD tests were performed after a significant ANOVA; Games-Howell tests were used after a significant Welch's ANOVA, and Dunn's tests with Holm's correction were carried out after any significant Kruskal-Wallis test. When comparisons against a zero-variance group (all observations having the same value) needed to be performed, one-sample *t*-tests were employed. Only when specified were a priori two-sample Mann-Whitney's tests performed. In the two latter cases, these tests are labelled in each plot with a lower-case letter if significant. When testing the effect of two factors, linear models were employed. For models involving independent observations and fixed factors, the generalized least squares approximation (GLS implementation in the R package nlme) was used. Conversely, for models involving repeated measures, linear mixed effects models were fitted using the lme implementation in the R package nlme. Unless otherwise specified, time, treatment and their interaction were included in the model as fixed factors, and the experimental subject was considered a random factor. The corresponding random intercept models were fitted to the data using restricted maximum likelihood. Importantly, the correlation between longitudinal observations as well as heteroskedasticity were included in the model when required. For both modelling approaches, assumptions were tested graphically (using quantile-quantile and residual plots), and model selection was based on likelihood ratio tests. For pairwise comparisons of the significant terms, estimated marginal means were calculated and compared using the R package emmeans, correcting for multiple testing using the multivariate *t*-distribution adjustment when needed. Finally, survival analyses were performed to test the differences in clinical signs and mortality using Kaplan-Meier estimates and the log-rank test. Statistically significant differences between groups are indicated with a line on top of each group: ** $p<0.01$; * $p<0.05$; $^{+}$ $0.05<p<0.1$.

KEY RESOURCES TABLE: See attached document.

9. Supplemental Information: See attached document.

10. References

Alanagreh, L., Alzoughool, F., Atoum, M., 2020. The Human Coronavirus Disease COVID-19: Its Origin, Characteristics, and Insights into Potential Drugs and Its Mechanisms. Pathogens 9, 331. https://doi.org/10.3390/pathogens9050331

An, Y., Li, S., Jin, X., Han, J., Xu, K., Xu, S., Han, Y., Liu, C., Zheng, T., Liu, M., Yang, M., Song, T., Huang, B., Zhao, L., Wang, W., Ruhan, A., Cheng, Y., Wu, C., Huang, E., Yang, S., Wong, G., Bi, Y., Ke, C., Tan, W., Yan, J., Zheng, Y., Dai, L., Gao, G.F., 2021. A tandem-repeat dimeric RBD protein-based COVID-19 vaccine ZF2001 protects mice and nonhuman primates. bioRxiv 2021.03.11.434928. https://doi.org/10.1101/2021.03.11.434928

Brustolin, M., Rodon, J., de la Concepción, M.L.R., Ávila-Nieto, C., Cantero, G., Pérez, M., Te, N., Noguera-Julián, M., Guallar, V., Valencia, A., Roca, N., Izquierdo-Useros, N., Blanco, J., Clotet, B., Bensaid, A., Carrillo, J., Vergara-Alert, J., Segalés, J., 2021a. Protection against reinfection with D614- or G614-SARS-CoV-2 isolates in golden Syrian hamster. Emerging Microbes & Infections 10, 797–809. https://doi.org/10.1080/22221751.2021.1913974

Cao, Y., Wang, J., Jian, F., Xiao, T., Song, W., Yisimayi, A., Huang, W., Li, Q., Wang, P., An, R., Wang, J., Wang, Yao, Niu, X., Yang, S., Liang, H., Sun, H., Li, T., Yu, Y., Cui, Q., Liu, S., Yang, X., Du, S., Zhang, Z., Hao, X., Shao, F., Jin, R., Wang, X., Xiao, J., Wang, Youchun, Xie, X.S., 2022. Omicron escapes the majority of existing SARS-CoV-2 neutralizing antibodies. Nature 602, 657–663. https://doi.org/10.1038/s41586-021-04385-3

Comirnaty smpc 2021, n.d. https://www.ema.europa.eu/en/documents/product-information/comirnaty-epar-product-information_en.pdf. .

Corman, V.M., Landt, O., Kaiser, M., Molenkamp, R., Meijer, A., Chu, D.K.W., Bleicker, T., Brünink, S., Schneider, J., Schmidt, M.L., Mulders, D.G.J.C., Haagmans, B.L., van der Veer, B., van den Brink, S., Wijsman, L., Goderski, G., Romette, J.L., Ellis, J., Zambon, M., Peiris, M., Goossens, H., Reusken, C., Koopmans, M.P.G., Drosten, C., 2020. Detection of 2019 novel coronavirus (2019-nCoV) by real-time RT-PCR. Eurosurveillance 25. https://doi.org/10.2807/1560-7917.ES.2020.25.3.2000045

Dai, L., Gao, G.F., 2021. Viral targets for vaccines against COVID-19. Nature Reviews Immunology 21, 73–82. https://doi.org/10.1038/s41577-020-00480-0

Francica, J.R., Flynn, B.J., Foulds, K.E., Noe, A.T., Werner, A.P., Moore, I.N., Gagne, M., Johnston, T.S., Tucker, C., Davis, R.L., Flach, B., O'Connell, S., Andrew, S.F., Lamb, E., Flebbe, D.R., Nurmukhambetova, S.T., Donaldson, M.M., Todd, J.-P.M., Zhu, A.L., Atyeo, C., Fischinger, S., Gorman, M.J., Shin, S., Edara, V.V., Floyd, K., Lai, L., Tylor, A., McCarthy, E., Lecouturier, V., Ruiz, S., Berry, C., Tibbitts, T., Andersen, H., Cook, A., Dodson, A., Pessaint, L., Ry, A. van, Koutsoukos, M., Gutzeit, C., Teng, I.-T., Zhou, T., Li, D., Haynes, B.F., Kwong, P.D., McDermott, A., Lewis, M.G., Fu, T.M., Chicz, R., van der Most, R., Corbett, K.S., Suthar, M.S., Alter, G., Roederer, M., Sullivan, N.J., Douek, D.C., Graham, B.S., Casimiro, D., Seder, R.A., 2021. Vaccination with SARS-CoV-2 Spike Protein and AS03 Adjuvant Induces Rapid Anamnestic Antibodies in the Lung and Protects Against Virus Challenge in Nonhuman Primates. bioRxiv 2021.03.02.433390. https://doi.org/10.1101/2021.03.02.433390

Garcia-Beltran, W.F., Lam, E.C., st. Denis, K., Nitido, A.D., Garcia, Z.H., Hauser, B.M., Feldman, J., Pavlovic, M.N., Gregory, D.J., Poznansky, M.C., Sigal, A., Schmidt, A.G., Iafrate, A.J., Naranbhai, V., Balazs, A.B., 2021. Multiple SARS-CoV-2 variants escape neutralization by vaccine-induced humoral immunity. Cell 184, 2372-2383.e9. https://doi.org/10.1016/j.cell.2021.03.013

Gavi Alliance- Covax collaboration platform, 2021. "What are protein subunit vaccines and how could they be used against COVID-19?" [WWW Document].

Genomic epidemiology of novel coronavirus - Global subsampling, 2021. https://nextstrain.org/ncov/gisaid/global?d=frequencies&p=full [WWW Document].

Goepfert, P.A., Fu, B., Chabanon, A.-L., Bonaparte, M.I., Davis, M.G., Essink, B.J., Frank, I., Haney, O., Janosczyk, H., Keefer, M.C., Koutsoukos, M., Kimmel, M.A., Masotti, R., Savarino, S.J., Schuerman, L., Schwartz, H., Sher, L.D., Smith, J., Tavares-Da-Silva, F., Gurunathan, S., DiazGranados, C.A., de Bruyn, G., 2021. Safety and immunogenicity of SARS-CoV-2 recombinant protein vaccine formulations in healthy adults: interim results of a randomised, placebo-controlled, phase 1–2, dose-ranging study. The Lancet Infectious Diseases 21, 1257–1270. https://doi.org/10.1016/S1473-3099(21)00147-X

Greaney, Allison J., Loes, A.N., Crawford, K.H.D., Starr, T.N., Malone, K.D., Chu, H.Y., Bloom, J.D., 2021a. Comprehensive mapping of mutations in the SARS-CoV-2 receptor-binding domain that affect recognition by polyclonal human plasma antibodies. Cell Host and Microbe 29, 463-476.e6. https://doi.org/10.1016/j.chom.2021.02.003

Greaney, Allison J, Loes, A.N., Gentles, L.E., Crawford, K.H.D., Starr, T.N., Malone, K.D., Chu, H.Y., Bloom, J.D., 2021b. Antibodies elicited by mRNA-1273 vaccination bind more broadly to the receptor binding domain than do those from SARS-CoV-2 infection, Sci. Transl. Med.https://doi.org/10.1126/scitranslmed.abi9915

Günl, F., Mecate-Zambrano, A., Rehländer, S., Hinse, S., Ludwig, S., Brunotte, L., 2021a. Shooting at a moving target—effectiveness and emerging challenges for sars-cov-2 vaccine development. Vaccines (Basel). https://doi.org/10.3390/vaccines9101052

Hadfield, J., Megill, C., Bell, S.M., Huddleston, J., Potter, B., Callender, C., Sagulenko, P., Bedford, T., Neher, R.A., 2018. Nextstrain: real-time tracking of pathogen evolution. Bioinformatics 34, 4121–4123. https://doi.org/10.1093/bioinformatics/bty407

Hannah Ritchie, Edouard Mathieu, Lucas Rodés-Guirao, Cameron Appel, Charlie Giattino, Esteban Ortiz-Ospina, Joe Hasell, Bobbie Macdonald, Diana Beltekian, Max Roser, 2020. "Coronavirus Pandemic (COVID-19)" [WWW Document]. Published online at OurWorldInData.org.

Huang, Y., Yang, C., Xu, X., Xu, W., Liu, S., 2020. Structural and functional properties of SARS-CoV-2 spike protein: potential antivirus drug development for COVID-19. Acta Pharmacologica Sinica 41, 1141–1149. https://doi.org/10.1038/s41401-020-0485-4

Jangra, S., Ye, C., Rathnasinghe, R., Stadlbauer, D., Alshammary, H., Amoako, A.A., Awawda, M.H., Beach, K.F., Bermúdez-González, M.C., Chernet, R.L., Eaker, L.Q., Ferreri, E.D., Floda, D.L., Gleason, C.R., Kleiner, G., Jurczyszak, D., Matthews, J.C., Mendez, W.A., Mulder, L.C.F., Russo, K.T., Salimbangon, A.B.T., Saksena, M., Shin, A.S., Sominsky, L.A.,

Srivastava, K., Krammer, F., Simon, V., Martinez-Sobrido, L., García-Sastre, A., Schotsaert, M., 2021. SARS-CoV-2 spike E484K mutation reduces antibody neutralisation. The Lancet Microbe. https://doi.org/10.1016/S2666-5247(21)00068-9

Jcovden Smpc [WWW Document], n.d. URL https://www.ema.europa.eu/en/medicines/human/EPAR/jcovden-previously-covid-19-vaccine-janssen (accessed 5.31.22).

Keech, C., Albert, G., Cho, I., Robertson, A., Reed, P., Neal, S., Plested, J.S., Zhu, M., Cloney-Clark, S., Zhou, H., Smith, G., Patel, N., Frieman, M.B., Haupt, R.E., Logue, J., McGrath, M., Weston, S., Piedra, P.A., Desai, C., Callahan, K., Lewis, M., Price-Abbott, P., Formica, N., Shinde, V., Fries, L., Lickliter, J.D., Griffin, P., Wilkinson, B., Glenn, G.M., 2020. Phase 1–2 Trial of a SARS-CoV-2 Recombinant Spike Protein Nanoparticle Vaccine. New England Journal of Medicine 383, 2320–2332. https://doi.org/10.1056/NEJMoa2026920

Kleanthous, H., Silverman, J.M., Makar, K.W., Yoon, I.-K., Jackson, N., Vaughn, D.W., 2021. Scientific rationale for developing potent RBD-based vaccines targeting COVID-19. npj Vaccines 6, 128. https://doi.org/10.1038/s41541-021-00393-6

Kuo, T.-Y., Lin, M.-Y., Coffman, R.L., Campbell, J.D., Traquina, P., Lin, Y.-J., Liu, L.T.-C., Cheng, J., Wu, Y.-C., Wu, C.-C., Tang, W.-H., Huang, C.-G., Tsao, K.-C., Chen, C., 2020. Development of CpG-adjuvanted stable prefusion SARS-CoV-2 spike antigen as a subunit vaccine against COVID-19. Scientific Reports 10, 20085. https://doi.org/10.1038/s41598-020-77077-z

Kyriakidis, N.C., López-Cortés, A., González, E.V., Grimaldos, A.B., Prado, E.O., 2021. SARS-CoV-2 vaccines strategies: a comprehensive review of phase 3 candidates. npj Vaccines 6, 28. https://doi.org/10.1038/s41541-021-00292-w

Lee, W.S., Wheatley, A.K., Kent, S.J., DeKosky, B.J., 2020. Antibody-dependent enhancement and SARS-CoV-2 vaccines and therapies. Nature Microbiology 5, 1185–1191. https://doi.org/10.1038/s41564-020-00789-5

Liu, Z., Xu, W., Xia, S., Gu, C., Wang, X., Wang, Q., Zhou, J., Wu, Y., Cai, X., Qu, D., Ying, T., Xie, Y., Lu, L., Yuan, Z., Jiang, S., 2020. RBD-Fc-based COVID-19 vaccine candidate induces highly potent SARS-CoV-2 neutralizing antibody response. Signal Transduction and Targeted Therapy 5. https://doi.org/10.1038/s41392-020-00402-5

Mathieu, E., Ritchie, H., Ortiz-Ospina, E., Roser, M., Hasell, J., Appel, C., Giattino, C., Rodés-Guirao, L., 2021. Author Correction: A global database of COVID-19 vaccinations. Nature Human Behaviour 5, 956–959. https://doi.org/10.1038/s41562-021-01160-2

Mellet, J., Pepper, M.S., 2021. A covid-19 vaccine: Big strides come with big challenges. Vaccines (Basel). https://doi.org/10.3390/vaccines9010039

Moyo-Gwete, T., Madzivhandila, M., Makhado, Z., Ayres, F., Mhlanga, D., Oosthuysen, B., Lambson, B.E., Kgagudi, P., Tegally, H., Iranzadeh, A., Doolabh, D., Tyers, L., Chinhoyi, L.R., Mennen, M., Skelem, S., Marais, G., Wibmer, C.K., Bhiman, J.N., Ueckermann, V., Rossouw, T., Boswell, M., de Oliveira, T., Williamson, C., Burgers, W.A., Ntusi, N., Morris, L., Moore, P.L., 2021a. SARS-CoV-2 501Y.V2 (B.1.351) elicits cross-reactive neutralizing antibodies. bioRxiv 2021.03.06.434193. https://doi.org/10.1101/2021.03.06.434193

Pallesen, J., Wang, N., Corbett, K.S., Wrapp, D., Kirchdoerfer, R.N., Turner, H.L., Cottrell, C.A., Becker, M.M., Wang, L., Shi, W., Kong, W.-P., Andres, E.L., Kettenbach, A.N., Denison, M.R., Chappell, J.D., Graham, B.S., Ward, A.B., McLellan, J.S., 2017. Immunogenicity and structures of a rationally designed prefusion MERS-CoV spike antigen. Proceedings of the National Academy of Sciences 114, E7348–E7357. https://doi.org/10.1073/pnas.1707304114

Pettersen, E.F., Goddard, T.D., Huang, C.C., Meng, E.C., Couch, G.S., Croll, T.I., Morris, J.H., Ferrin, T.E., 2021. <scp>UCSF ChimeraX</scp> : Structure visualization for researchers, educators, and developers. Protein Science 30, 70–82. https://doi.org/10.1002/pro.3943

Piccoli, L., Park, Y.-J., Tortorici, M.A., Czudnochowski, N., Walls, A.C., Beltramello, M., Silacci-Fregni, C., Pinto, D., Rosen, L.E., Bowen, J.E., Acton, O.J., Jaconi, S., Guarino, B., Minola, A., Zatta, F., Sprugasci, N., Bassi, J., Peter, A., de Marco, A., Nix, J.C., Mele, F., Jovic, S., Rodriguez, B.F., Gupta, S. v., Jin, F., Piumatti, G., lo Presti, G., Pellanda, A.F., Biggiogero, M., Tarkowski, M., Pizzuto, M.S., Cameroni, E., Havenar-Daughton, C., Smithey, M., Hong, D., Lepori, V., Albanese, E., Ceschi, A., Bernasconi, E., Elzi, L., Ferrari, P., Garzoni, C., Riva, A., Snell, G., Sallusto, F., Fink, K., Virgin, H.W., Lanzavecchia, A., Corti, D., Veesler, D., 2020. Mapping Neutralizing and Immunodominant Sites on the SARS-CoV-2 Spike Receptor-Binding Domain by Structure-Guided High-Resolution Serology. Cell 183, 1024-1042.e21. https://doi.org/10.1016/j.cell.2020.09.037

Planas, D., Veyer, D., Baidaliuk, A., Staropoli, I., Guivel-Benhassine, F., Rajah, M.M., Planchais, C., Porrot, F., Robillard, N., Puech, J., Prot, M., Gallais, F., Gantner, P., Velay, A., le Guen, J., Kassis-Chikhani, N., Edriss, D., Belec, L., Seve, A., Courtellemont, L., Péré, H., Hocqueloux, L., Fafi-Kremer, S., Prazuck, T., Mouquet, H., Bruel, T., Simon-Lorière, E., Rey, F.A., Schwartz, O., 2021. Reduced sensitivity of SARS-CoV-2 variant Delta to antibody neutralization. Nature 596, 276–280. https://doi.org/10.1038/s41586-021-03777-9

Plante, J.A., Mitchell, B.M., Plante, K.S., Debbink, K., Weaver, S.C., Menachery, V.D., 2021. The variant gambit: COVID-19's next move. Cell Host & Microbe 29, 508–515. https://doi.org/10.1016/j.chom.2021.02.020

Pradenas, E., Trinité, B., Urrea, V., Marfil, S., Ávila-Nieto, C., Rodríguez de la Concepción, M.L., Tarrés-Freixas, F., Pérez-Yanes, S., Rovirosa, C., Ainsua-Enrich, E., Rodon, J., Vergara-Alert, J., Segalés, J., Guallar, V., Valencia, A., Izquierdo-Useros, N., Paredes, R., Mateu, L., Chamorro, A., Massanella, M., Carrillo, J., Clotet, B., Blanco, J., 2021. Stable neutralizing antibody levels 6 months after mild and severe COVID-19 episodes. Med 2, 313-320.e4. https://doi.org/10.1016/j.medj.2021.01.005

Ramanathan, M., Ferguson, I.D., Miao, W., Khavari, P.A., 2021. SARS-CoV-2 B.1.1.7 and B.1.351 spike variants bind human ACE2 with increased affinity. The Lancet Infectious Diseases 21, 1070. https://doi.org/10.1016/S1473-3099(21)00262-0

Rodon, J., Okba, N.M.A., Te, N., van Dieren, B., Bosch, B.J., Bensaid, A., Segalés, J., Haagmans, B.L., Vergara-Alert, J., 2019. Blocking transmission of Middle East respiratory syndrome coronavirus (MERS-CoV) in llamas by vaccination with a recombinant spike protein. Emerging Microbes and Infections 8, 1593–1603. https://doi.org/10.1080/22221751.2019.1685912

Sharker, S.Md., Rahman, A., 2021. A Review on the Current Methods of Chinese Hamster Ovary (CHO) Cells Cultivation for the Production of Therapeutic Protein. Current Drug Discovery Technologies 18, 354–364. https://doi.org/10.2174/1570163817666200312102137

Snapper, C.M., Paul, W.E., 1987. Interferon-γ and B Cell Stimulatory Factor-1 Reciprocally Regulate Ig Isotype Production. Science (1979) 236, 944–947. https://doi.org/10.1126/science.3107127

Spellberg, B., Edwards, J.E., 2001. Type 1/Type 2 Immunity in Infectious Diseases. Clinical Infectious Diseases 32, 76–102. https://doi.org/10.1086/317537

Spikevax Smpc, 2021. https://www.ema.europa.eu/en/documents/product-information/spikevax-previously-covid-19-vaccine-moderna-epar-product-information_en.pdf.

Tian, J.-H., Patel, N., Haupt, R., Zhou, H., Weston, S., Hammond, H., Logue, J., Portnoff, A.D., Norton, J., Guebre-Xabier, M., Zhou, B., Jacobson, K., Maciejewski, S., Khatoon, R., Wisniewska, M., Moffitt, W., Kluepfel-Stahl, S., Ekechukwu, B., Papin, J., Boddapati, S., Jason Wong, C., Piedra, P.A., Frieman, M.B., Massare, M.J., Fries, L., Bengtsson, K.L., Stertman, L., Ellingsworth, L., Glenn, G., Smith, G., 2021. SARS-CoV-2 spike glycoprotein vaccine candidate NVX-CoV2373 immunogenicity in baboons and protection in mice. Nature Communications 12, 372. https://doi.org/10.1038/s41467-020-20653-8

Trinité, B., Tarrés-Freixas, F., Rodon, J., Pradenas, E., Urrea, V., Marfil, S., Rodríguez de la Concepción, M.L., Ávila-Nieto, C., Aguilar-Gurrieri, C., Barajas, A., Ortiz, R., Paredes, R., Mateu, L., Valencia, A., Guallar, V., Ruiz, L., Grau, E., Massanella, M., Puig, J., Chamorro, A., Izquierdo-Useros, N., Segalés, J., Clotet, B., Carrillo, J., Vergara-Alert, J., Blanco, J., 2021b. SARS-CoV-2 infection elicits a rapid neutralizing antibody response that correlates with disease severity. Scientific Reports 11, 2608. https://doi.org/10.1038/s41598-021-81862-9

U.S. National Library of Medicine, 2021. Safety and Immunogenicity Study of Recombinant Protein RBD Candidate Vaccine Against SARS-CoV-2 in Adult Healthy Volunteers (COVID-19). Identifier: NCT05007509. Available at: https://www.clinicaltrials.gov/ct2/show/NCT05007509.”.

Vergara-Alert, J., van den Brand, J.M.A., Widagdo, W., Muñoz, M., Raj, V.S., Schipper, D., Solanes, D., Cordón, I., Bensaid, A., Haagmans, B.L., Segalés, J., 2017. Livestock susceptibility to infection with middle east respiratory syndrome coronavirus. Emerging Infectious Diseases 23, 232–240. https://doi.org/10.3201/eid2302.161239

Vidal, E., López-Figueroa, C., Rodon, J., Pérez, M., Brustolin, M., Cantero, G., Guallar, V., Izquierdo-Useros, N., Carrillo, J., Blanco, J., Clotet, B., Vergara-Alert, J., Segalés, J., 2021b. Chronological brain lesions after SARS-CoV-2 infection in hACE2-transgenic mice. Veterinary Pathology. https://doi.org/10.1177/03009858211066841

Vogel, A.B., Kanevsky, I., Che, Y., Swanson, K.A., Muik, A., Vormehr, M., Kranz, L.M., Walzer, K.C., Hein, S., Güler, A., Loschko, J., Maddur, M.S., Tompkins, K., Cole, J., Lui, B.G., Ziegenhals, T., Plaschke, A., Eisel, D., Dany, S.C., Fesser, S., Erbar, S., Bates, F., Schneider, D., Jesionek, B., Sänger, B., Wallisch, A.-K., Feuchter, Y., Junginger, H., Krumm, S.A.,

Heinen, A.P., Adams-Quack, P., Schlereth, J., Kröner, C., Hall-Ursone, S., Brasky, K., Griffor, M.C., Han, S., Lees, J.A., Mashalidis, E.H., Sahasrabudhe, P. v, Tan, C.Y., Pavliakova, D., Singh, G., Fontes-Garfias, C., Pride, M., Scully, I.L., Ciolino, T., Obregon, J., Gazi, M., Carrion, R., Alfson, K.J., Kalina, W. v, Kaushal, D., Shi, P.-Y., Klamp, T., Rosenbaum, C., Kuhn, A.N., Türeci, Ö., Dormitzer, P.R., Jansen, K.U., Sahin, U., 2020. A prefusion SARS-CoV-2 spike RNA vaccine is highly immunogenic and prevents lung infection in non-human primates. bioRxiv 2020.09.08.280818. https://doi.org/10.1101/2020.09.08.280818

Wall, E.C., Wu, M., Harvey, R., Kelly, G., Warchal, S., Sawyer, C., Daniels, R., Hobson, P., Hatipoglu, E., Ngai, Y., Hussain, S., Nicod, J., Goldstone, R., Ambrose, K., Hindmarsh, S., Beale, R., Riddell, A., Gamblin, S., Howell, M., Kassiotis, G., Libri, V., Williams, B., Swanton, C., Gandhi, S., Bauer, D.L., 2021. Neutralising antibody activity against SARS-CoV-2 VOCs B.1.617.2 and B.1.351 by BNT162b2 vaccination. The Lancet 397, 2331–2333. https://doi.org/10.1016/S0140-6736(21)01290-3

Wang, H., Wu, X., Zhang, X., Hou, X., Liang, T., Wang, D., Teng, F., Dai, J., Duan, H., Guo, S., Li, Y., Yu, X., 2020. SARS-CoV-2 Proteome Microarray for Mapping COVID-19 Antibody Interactions at Amino Acid Resolution. ACS Central Science 6, 2238–2249. https://doi.org/10.1021/acscentsci.0c00742

WHO, 2021. WHO Coronavirus (COVID-19) Dashboard [WWW Document]. https://covid19.who.int/.

WHO 2022, n.d. Tracking SARS-CoV-2 variants [WWW Document].

Yi, C., Sun, X., Ye, J., Ding, L., Liu, M., Yang, Z., Lu, X., Zhang, Y., Ma, L., Gu, W., Qu, A., Xu, J., Shi, Z., Ling, Z., Sun, B., 2020. Key residues of the receptor binding motif in the spike protein of SARS-CoV-2 that interact with ACE2 and neutralizing antibodies. Cellular & Molecular Immunology 17, 621–630. https://doi.org/10.1038/s41423-020-0458-z

Zhou, P., Yang, X.-L., Wang, X.-G., Hu, B., Zhang, L., Zhang, W., Si, H.-R., Zhu, Y., Li, B., Huang, C.-L., Chen, H.-D., Chen, J., Luo, Y., Guo, H., Jiang, R.-D., Liu, M.-Q., Chen, Y., Shen, X.-R., Wang, X., Zheng, X.-S., Zhao, K., Chen, Q.-J., Deng, F., Liu, L.-L., Yan, B., Zhan, F.-X., Wang, Y.-Y., Xiao, G.-F., Shi, Z.-L., 2020. A pneumonia outbreak associated with a new coronavirus of probable bat origin. Nature 579, 270–273. https://doi.org/10.1038/s41586-020-2012-7

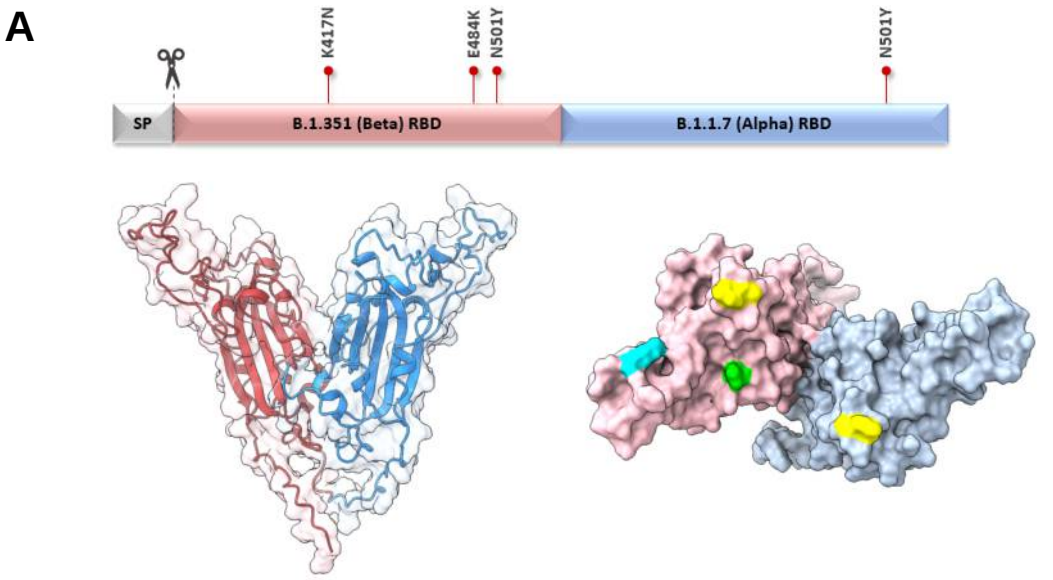

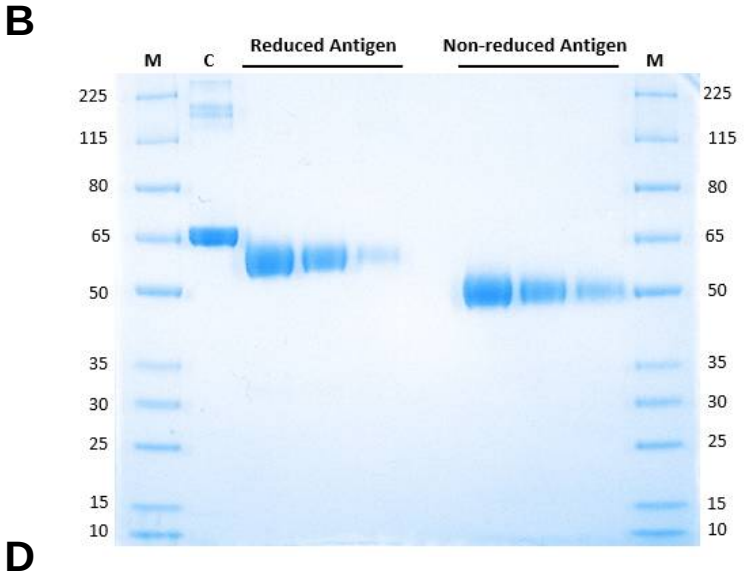

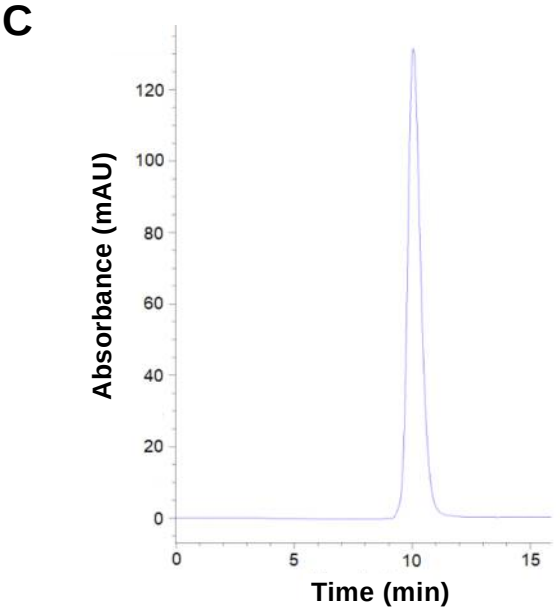

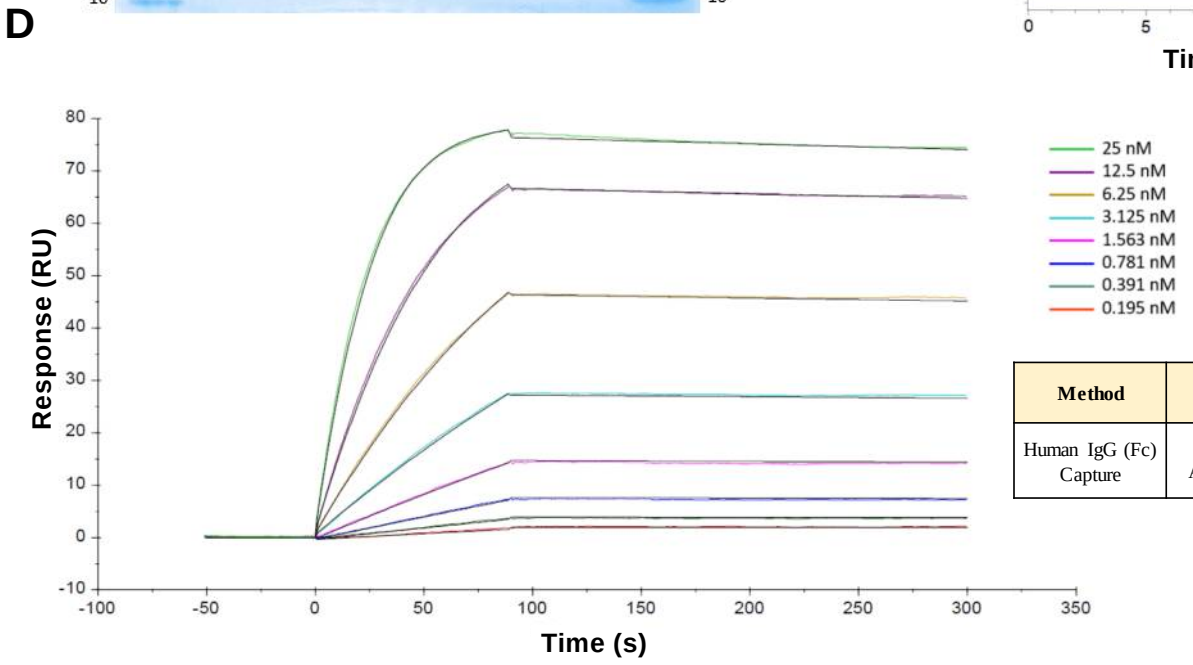

Method	Ligand	K_D (M)
Human IgG (Fc) Capture	Human ACE2 / ACEH Protein, Fc Tag	**9.85E-11**

Figure 1.

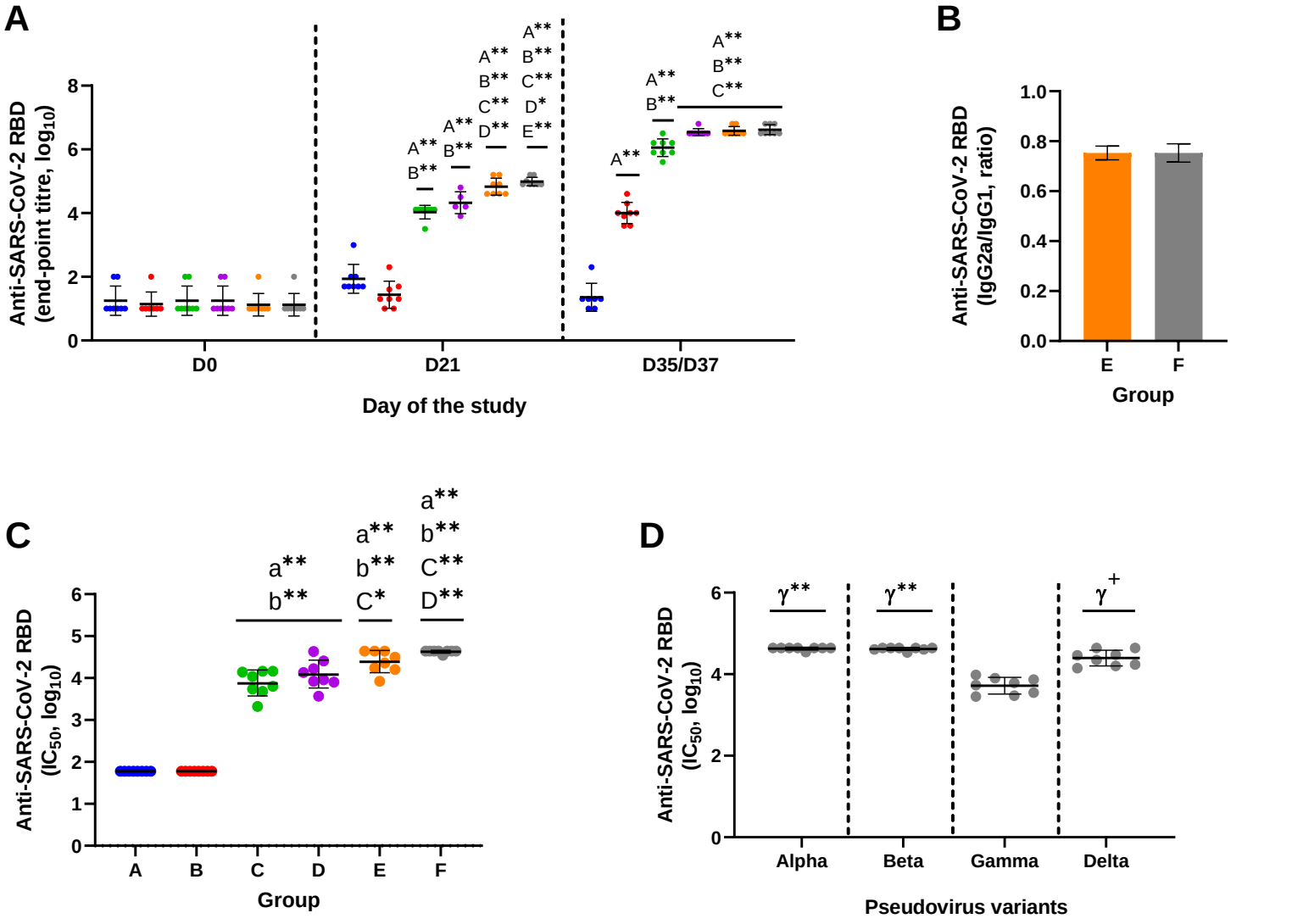

- A: Control (PBS)
- B: PHH-1V (0.04 µg RBD fusion heterodimer/dose)
- C: PHH-1V (0.2 µg RBD fusion heterodimer/dose)
- D: PHH-1V (1 µg RBD fusion heterodimer/dose)
- E: PHH-1V (5 µg RBD fusion heterodimer/dose)
- F: PHH-1V (20 µg RBD fusion heterodimer/dose)

Figure 2.

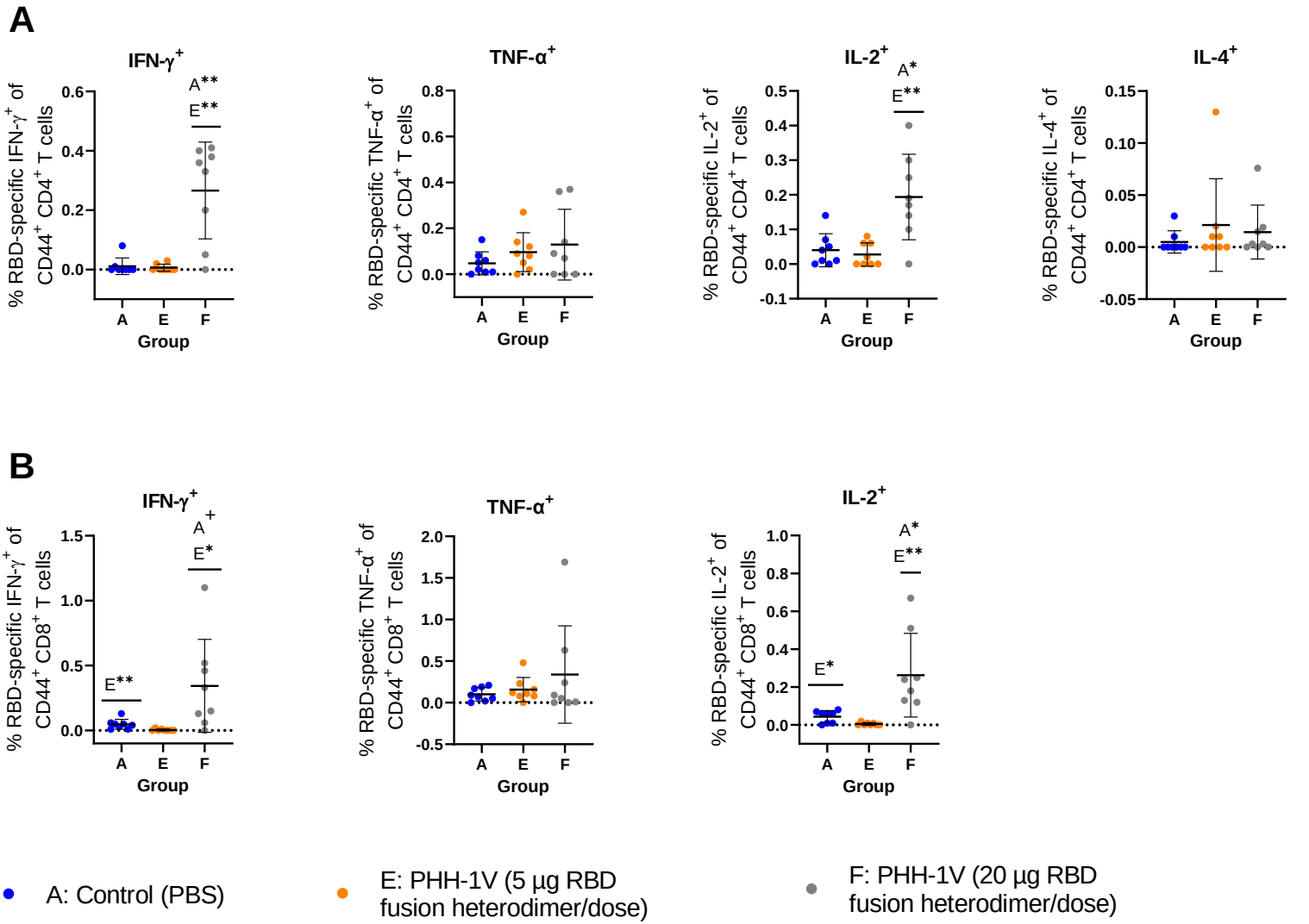
A
IFN-γ+
% RBD-specific IFN-γ+ of CD44+ CD4+ T cells
A**
E**
TNF-α+
% RBD-specific TNF-α+ of CD44+ CD4+ T cells
IL-2+
% RBD-specific IL-2+ of CD44+ CD4+ T cells
A*
E**
IL-4+
% RBD-specific IL-4+ of CD44+ CD4+ T cells
Group
A
E
F
B
IFN-γ+
% RBD-specific IFN-γ+ of CD44+ CD8+ T cells
A+
E*
E**
TNF-α+
% RBD-specific TNF-α+ of CD44+ CD8+ T cells
IL-2+
% RBD-specific IL-2+ of CD44+ CD8+ T cells
A*
E**
E*
A: Control (PBS)
E: PHH-1V (5 µg RBD fusion heterodimer/dose)
F: PHH-1V (20 µg RBD fusion heterodimer/dose)

Figure 3.

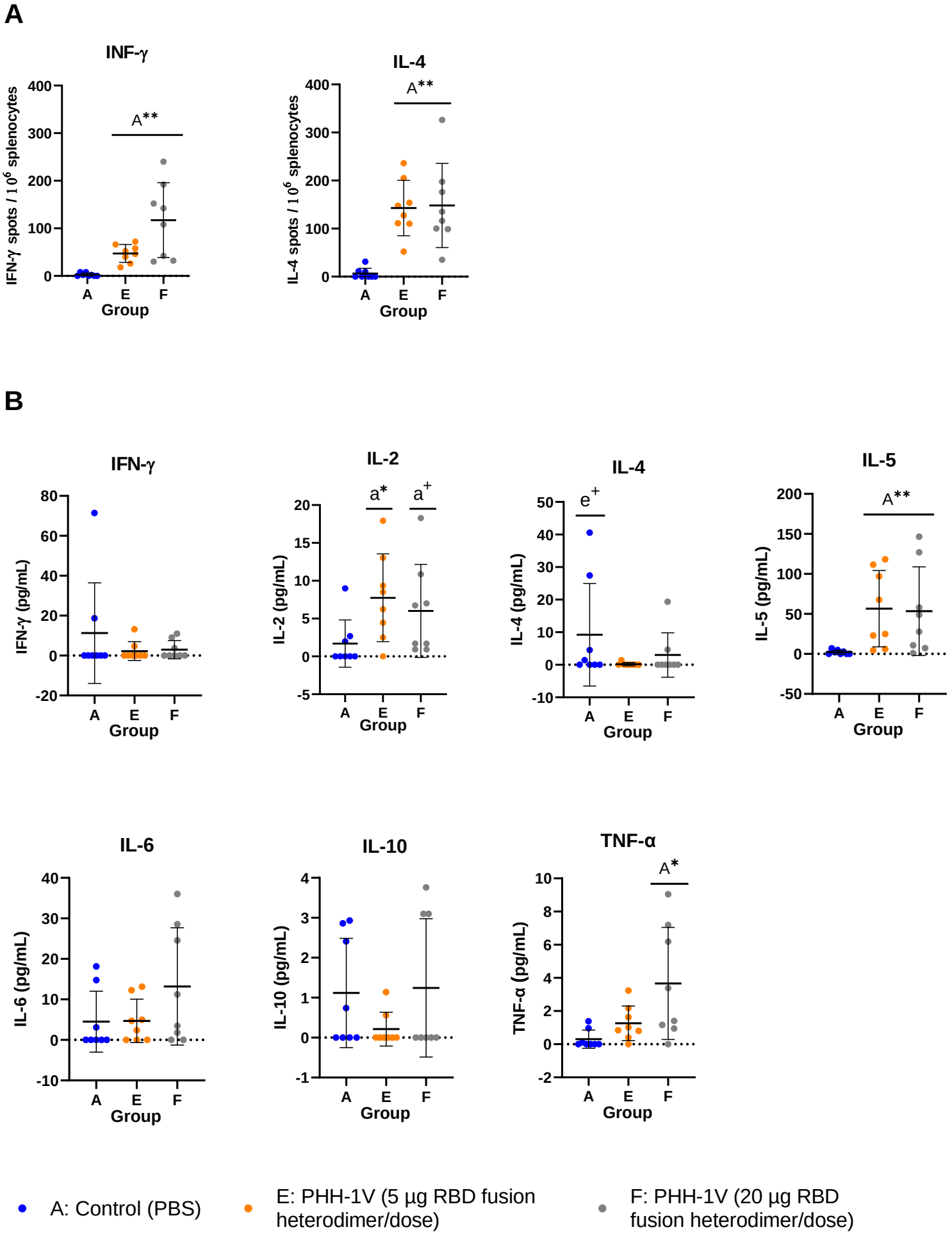
A
INF-γ
IFN-γ spots / 10^6 splenocytes
A**
IL-4
IL-4 spots / 10^6 splenocytes
A**
Group
B
IFN-γ
IFN-γ (pg/mL)
IL-2
IL-2 (pg/mL)
a*
a+
IL-4
IL-4 (pg/mL)
e+
IL-5
IL-5 (pg/mL)
A**
IL-6
IL-6 (pg/mL)
IL-10
IL-10 (pg/mL)
TNF-α
TNF-α (pg/mL)
A*
A
E
F
Group
A: Control (PBS)
E: PHH-1V (5 µg RBD fusion heterodimer/dose)
F: PHH-1V (20 µg RBD fusion heterodimer/dose)

Figure 4.

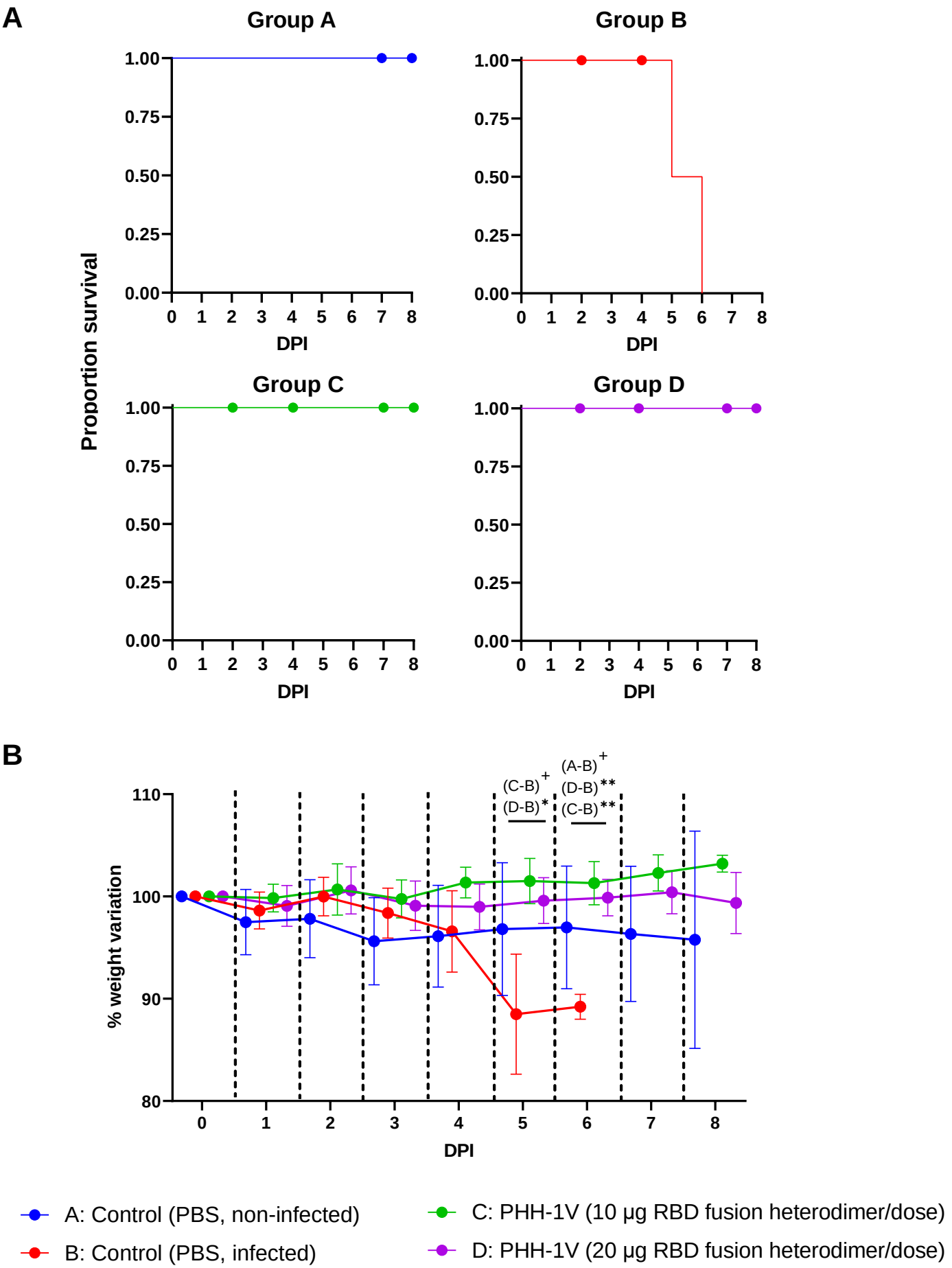
A
Group A
Group B
Group C
Group D
Proportion survival
1.00
0.75
0.50
0.25
0.00
0 1 2 3 4 5 6 7 8
DPI
B
% weight variation
110
100
90
80
(C-B)+
(D-B)*
(A-B)+
(D-B)**
(C-B)**
A: Control (PBS, non-infected)
B: Control (PBS, infected)
C: PHH-1V (10 µg RBD fusion heterodimer/dose)
D: PHH-1V (20 µg RBD fusion heterodimer/dose)

Figure 5.

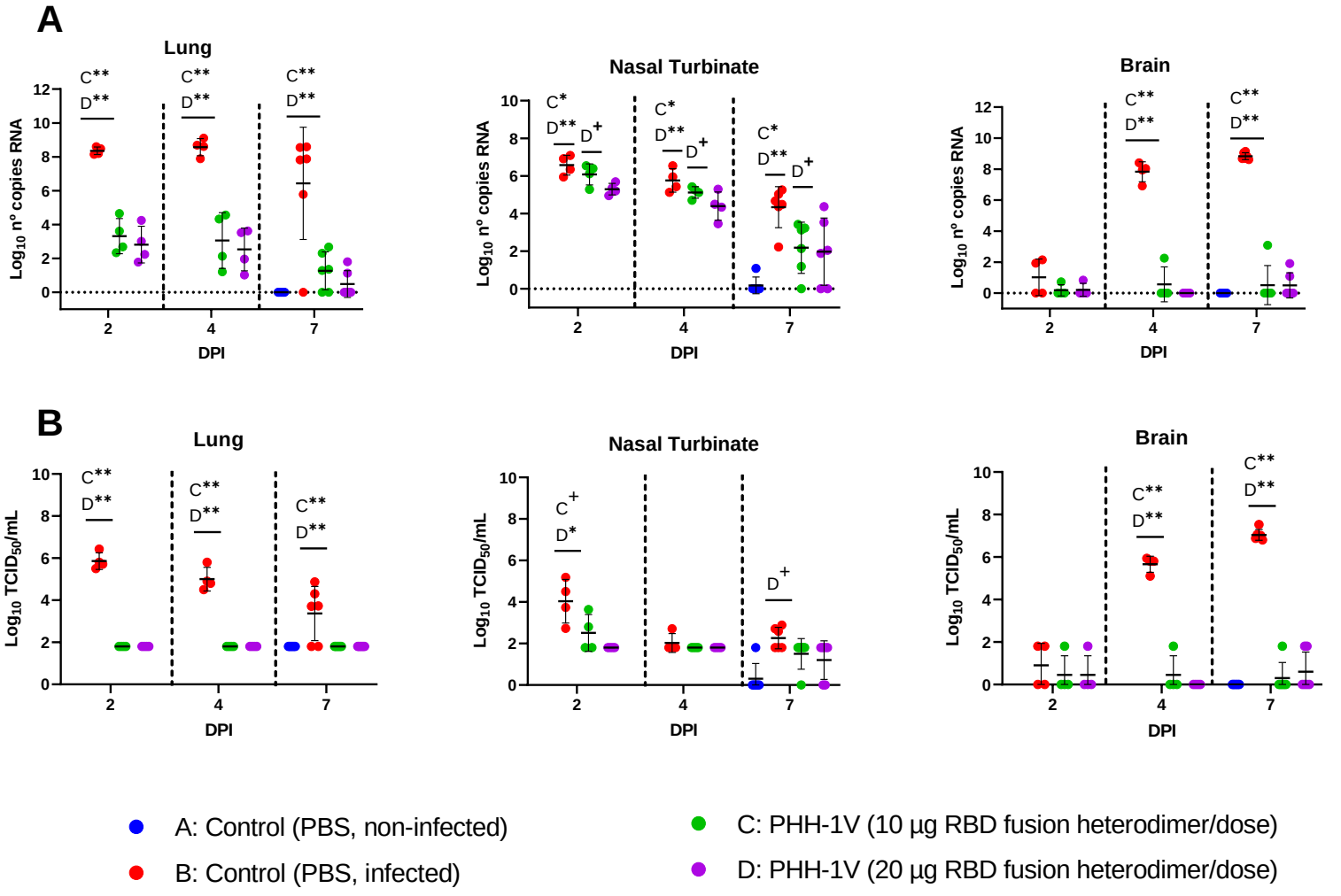
A
Lung
Nasal Turbinate
Brain
Log10 nº copies RNA
DPI
B
Log10 TCID50/mL
A: Control (PBS, non-infected)
B: Control (PBS, infected)
C: PHH-1V (10 µg RBD fusion heterodimer/dose)
D: PHH-1V (20 µg RBD fusion heterodimer/dose)

Figure 6.

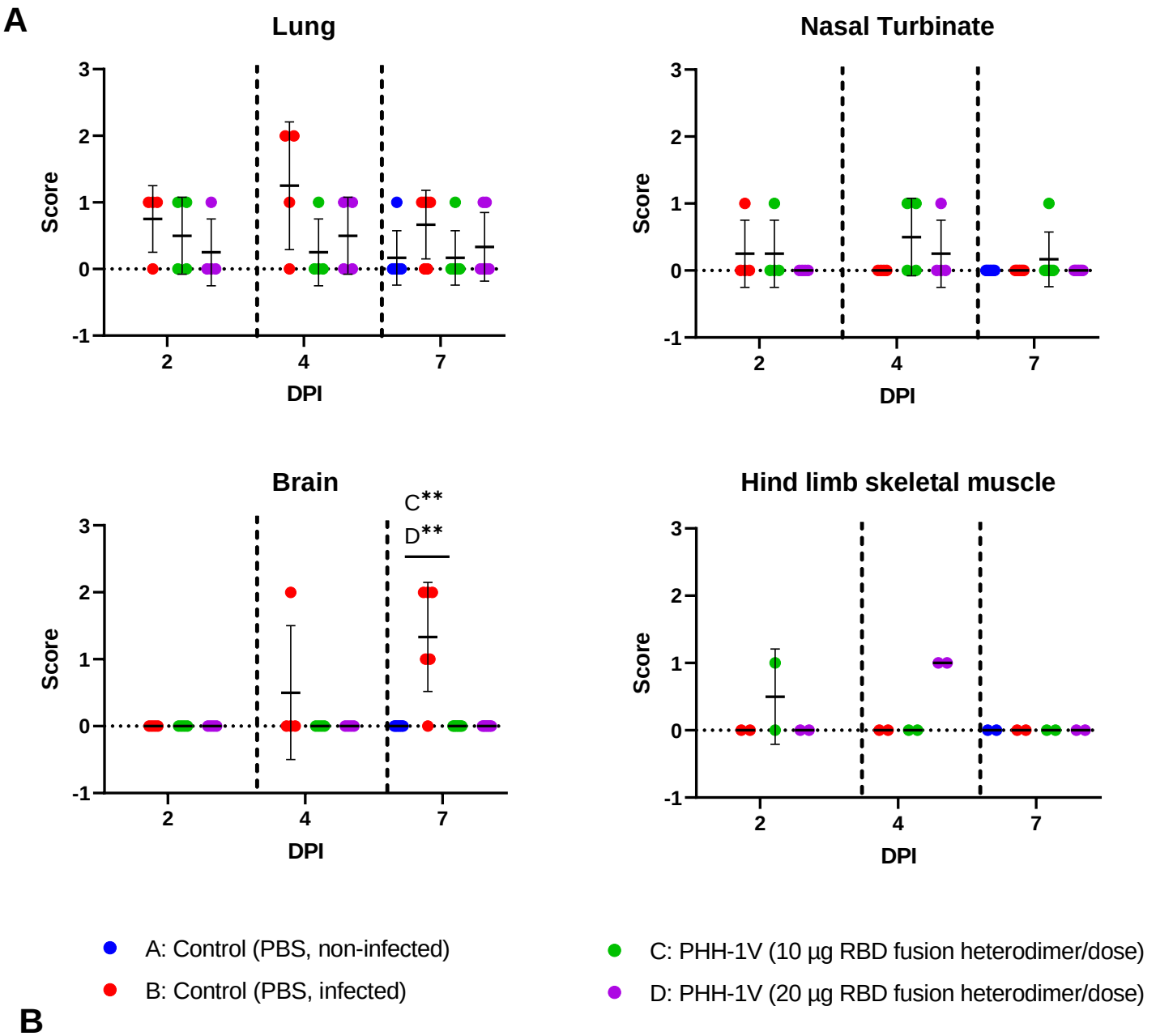
A
Lung
Nasal Turbinate
Brain
Hind limb skeletal muscle
Score
DPI
2
4
7
3
2
1
0
-1
C**
D**
A: Control (PBS, non-infected)
B: Control (PBS, infected)
C: PHH-1V (10 µg RBD fusion heterodimer/dose)
D: PHH-1V (20 µg RBD fusion heterodimer/dose)

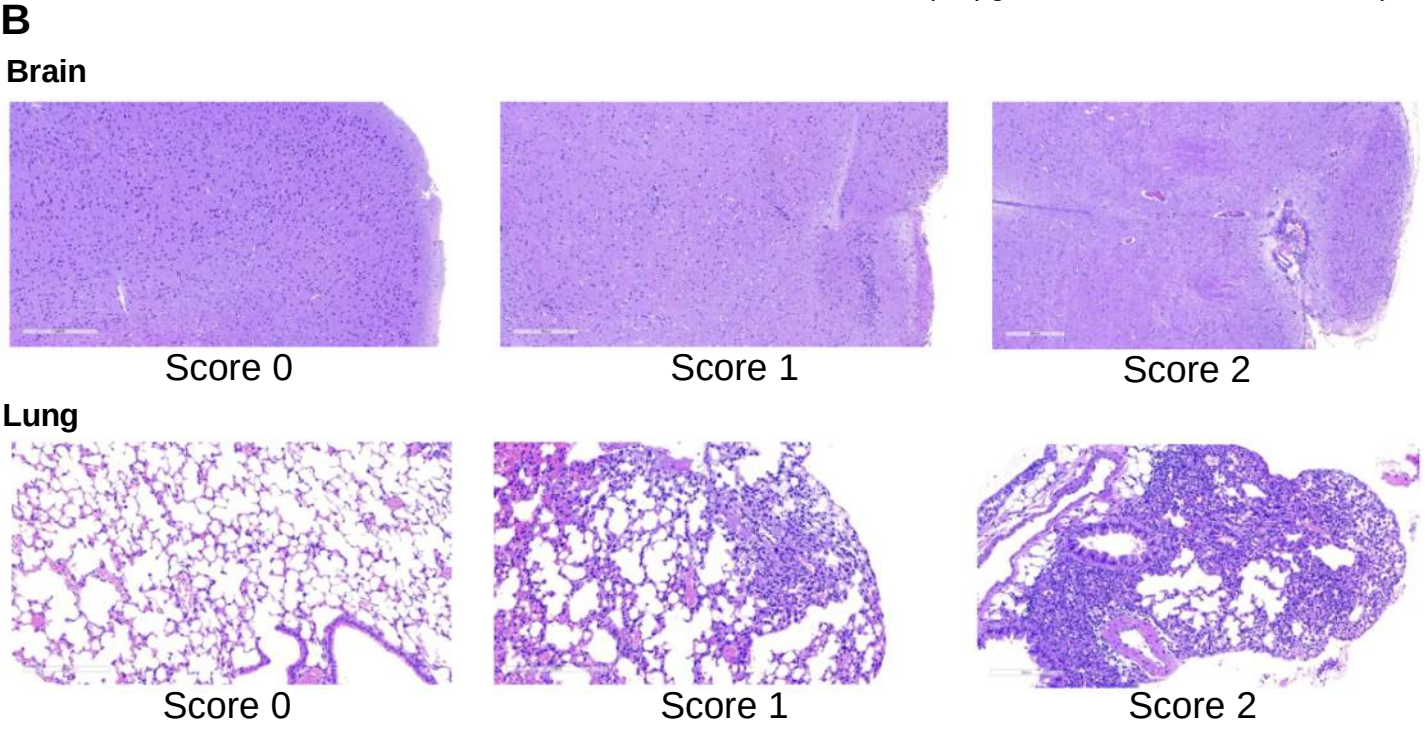
B
Brain
Score 0
Score 1
Score 2
Lung
Score 0
Score 1
Score 2

Figure 7.